Dissecting gene expression of single cells with reduced perturbation

SUBRAMANIAN PARIMALAM SANGAMITHIRAI

2021

Dissecting gene expression of single cells with reduced perturbation

A DISSERTATION

SUBMITTED TO THE DEPARTMENT OF

MICROENGINEERING AND

THE COMMITTEE OF GRADUATE STUDIES OF

KYOTO UNIVERSITY

IN PARTIAL FULFILMENT OF THE REQUIREMENTS FOR THE DEGREE

OF

DOCTOR OF PHILOSOPHY

SUBRAMANIAN PARIMALAM SANGAMITHIRAI

March 2021

Abstract

Gene expressions of single cells can be perturbed during sample collection, preparation, and adaptation for microfluidic protocols, resulting in distorted biological information. In this thesis, we developed two microfluidic approaches to measure gene expressions of single animal cells as well as plant cells at reduced perturbation. For animal cells, we employed a reversible crosslinking using dithiobis(succinimidyl propionate) (DSP) to "fix" the gene expression of cells at the time point of the fixation. We integrated the on-chip reverse crosslinking of DSP with electrical lysis leveraging focused field via a microfluidic geometry, isotachophoresis (ITP)-aided extraction of cytoplasmic RNA, and off-chip next-generation sequencing of cytoplasmic RNA. For single plant cells in an intact cluster, we designed a pulsed and focused electric field that selectively permeabilized the cell wall of a targeted cell in an intact plant cell cluster. We demonstrated the extraction of small molecules and RNA, the on-chip fluorescence measurement of the extracted molecules, and integration with off-chip reverse transcription-quantitative polymerase chain reaction (RT-qPCR) targeting mRNA in the extracted molecules.

To reduce perturbation in animal cells, we reported the development and modification of DSP-based fixation and its integration with our microfluidic approach. We made a crucial change to the DSP fixation protocol to maintain the integrity of the plasma membrane. We showed that our cell preservation protocol using 9.3% sucrose in the storage buffer significantly prolonged the integrity of the plasma membrane. This resulted in the retention of small molecules and reduced the leakage of RNA from fixed cells. Our new ITP chemistry enabled on-chip reverse crosslinking of fixed cells, electrical lysis of the plasma membrane, and ITP-aided RNA extraction from single DSP fixed cells. We exploited the focusing effect of the electrical field in the microfluidic system

to reduce the applied voltages and selectively lysed the plasma membrane of the fixed cell. We assessed the DSP fixation by comparing it to alternative fixation protocols using methanol and ethanol. We showed that the DSP fixation offered the highest efficiency of RNA extraction compared to the other fixation protocols. We demonstrated the integration of our approach with RNA-sequencing and critically benchmarked the sensitivity and repeatability. Gene expression analyses with extracted RNA from a single DSP-fixed cell displayed reduced repeatability and sensitivity compared to those with fresh cells, yet the averaged gene expression pattern was highly consistent with those of fresh cells. Unlike experiments with single fresh cells, cell fixation via DSP separates the sample collection from the downstream processing and enables coupling with the electrical lysis and extraction of RNA from fixed cells, allowing us to design complex studies.

To minimize perturbation in plant cells, we reported an approach to extract cytoplasmic molecules from an intact plant cell in a cluster using three-dimensional focusing of the electric field. To achieve three-dimensional focusing, we designed a microchannel integrated with a hydrodynamic trap (3 μm wide and 25 μm deep) and inlet channel with a larger cross-section (100 μm wide and 100 μm deep) than that of other parts of the microchannel (25 μm wide and 50 μm deep). This design effectively increased the local electric field at the hydrodynamic trap while significantly reduced in the inlet channel. We tested the approach by applying to two types of model plants (deep cells derived from the root cells from Arabidopsis thaliana and BY-2 cells of Nicotiana tabacum), which had distinct cluster morphologies, as well as a mammalian cell line (K562, human leukemia cell line), demonstrating the broad applicability of our microfluidic approach. We here evaluated the various conditions of the pulsed electric field by measuring the number of influenced cells in an intact cluster, identifying the influenced cells by propidium iodide (PI) staining after applying the pulsed voltage (before the application of the DC electric field). Our

data uncovered that both the intensity and the duration of the pulsed electric field were keys to control the number of influenced cells. We provided a landscape of conditions of the pulsed electric field for controlling the number of influenced cells in an intact cluster, where we characterized the conditions by the intensity and duration of the pulsed electric field at the hydrodynamic trap. To further confirm the extraction of RNA molecules, we performed off-chip RT-qPCR with the solution extracted from the outlet reservoir targeting *GAPC1*.

ACKNOWLEDGEMENTS

I express my gratitude to Dr. Hirofumi Shintaku for his constant guidance and support all throughout my time in his lab. I am so grateful for all the teachings, insights and pep talks he gave in shaping my research, education and overall personality. I am forever thankful to the opportunities you gave me.

I extend my sincere thanks to Emeritus Prof. Hidetoshi Kotera and Prof. Ryuji Yokokawa for their advice and encouragement. I had memorable experience at Kotera lab which I will cherish always.

Special thanks to the Government of Japan for granting me MEXT scholarship to pursue doctoral course.

I thank the thesis committee, Prof. Kazuyoshi Nakabe and Prof. Yasuhiro Inoue for kindly accepting to review my dissertation.

I thank all the administrative and technical staff members for their kindness and support. I appreciate all the collaborators at Kyoto University, RIKEN and the University of Tokyo for their inputs and contributions.

I convey my thanks to Mr. Takuya Waratani, for tutoring and helping me to make a smooth transition in the new lab environment during the initial days. I also extend my thanks to Dr. Mahmoud Nady Abdelmoez Atta, Mr. Arata Tsuchida, Dr. Taikopaul Kaneko and all the past and present lab members for their extraordinary support and cooperation.

I thank my family, host family and friends in Japan and India. Finally, I thank Japan for being so warm, welcoming and unique.

Table of contents

List of figures

LIST OF TABLES

1

Introduction

1.1 Background

Cellular heterogeneity is an inherent property of biological systems to address the various physiological requirements in both animal and plant species. It can be observed in isogenic populations of normal cells, stem cells, tumor cells and so on (Abdallah et al., 2013; Altschuler & Wu, 2010; Levy, 2016). Conventional approaches analyze cells using cellular contents extracted from large number of cells. During the process of bulk extraction of RNA, DNA and proteins, the cellular information from an individual cell is lost forever along any subpopulation information. They mask the underlying cellular heterogeneity that results in false and mis-leading information about the cell and cell population. It is therefore important to investigate cells at single cell level to understand the cellular events contributing to these dissimilarities (Darmanis et al., 2015; Wu et al., 2014). Tube based approaches may not be sensitive enough to analyze small quantities of analyte species and they also do not yield the high throughput required to analyze tens and thousands of single cells. To analyze single cells, miniature systems are required to increase the sensitivity of the analyte molecules in a single cell as they are present in the order of picograms. Hence, single-cell analysis is essential to understand cellular heterogeneity at molecular resolution (Elowitz, Levine, Siggia, & Swain, 2002; Newman et al., 2006; Raj & van Oudenaarden, 2008; Roy et al., 2018).

Recently, many microfluidics based single cell platforms like SINC-seq (Abdelmoez et al., 2018), microwell (Gierahn et al., 2017; Han et al., 2018), C1-fluidigm (Wu et al., 2014) and droplet (Macosko et al., 2015; Klein et al., 2015) based systems have been developed to increase the sensitivity, detectability and throughput to study the gene expression at single cell level. These technologies efficiently reduce the sample consumption and reaction time. They also allow effective manipulation of fluid flow and provide tightly regulated process environments. SINC-seq technology captures a single cell at a hydrodynamic trap and uses electric field to selectively lyse the plasma membrane of the single cell and fractionates the cytoplasmic and nuclear contents. Microwell based (Seq-well & microwell-seq) techniques analyses thousands of single cells by capturing them in picoliter to nanoliter volume wells. Here, each microwell acts an individual reaction chamber preserving the single cell information. C1-fluidigm is an integrated fluidic circuit that uses valves to control fluid flow in a microchannel, here a single cell is captured, lysed and the cell contents are prepped in a series of chambers for downstream analytical procedures. Droplet based (Drop-seq, inDrop and Chromium 10X) single cell techniques uses a two-phase liquid to create droplets where single cells are captured in single droplet and the droplet acts a compartment to sustain the cell contents. Single cell anlaysis has uncovered mechanisms leading to cellular heterogeneity, in cancer research (Navin, 2015; Tellez-Gabriel, Ory, Lamoureux, Heymann, & Heymann, 2016; Zhang et al., 2016), immunology (Jaitin et al., 2014; Papalexi & Satija, 2017; Shalek et al., 2013), neuron research (Darmanis et al., 2017; Darmanis et al., 2015), stem cell and developmental biology. They have also facilitated in establishing databases. Single cell analysis has also aided in the characterization of cell types and creation of cell atlas of different species uncovering novel cell types (Panina, Karagiannis, Kurtz, Stacey, & Fujibuchi, 2020; Saunders et al., 2018).

1.2 Multimodal omics in single cells

Cells are analyzed by targeting cell contents that can be broadly classified as genome, epi-genome, transcriptome, proteome and metabolome (Hu et al., 2018; Lee, Hyeon, & Hwang, 2020). Single cells technologies although initially were developed to analyze a single target in a cell have now evolved to analyze multiple targets from the same cell. Macaulay et al., (Macaulay et al., 2015) demonstrated simultaneous Genome and Transcriptome-seq (G&T-seq) using single cell isolated by flow cytometry. Here, a whole cell is lysed and the genomic DNA and mRNA are physically separated using magnetic beads for whole genome sequencing and single cell RNA sequencing. Angermueller et al., (Angermueller et al., 2016) used a similar whole cell lysis and bead based capture approach of anlaytes and performed a simultaneous analysis of single cell Methylome and Transcriptome sequencing (scM&T-seq). RNA Expression And Protein sequencing (REAP-seq) is a simultaneous detection technique of RNA and protein from the same single cell has been implemented on 10x genomics (Peterson et al., 2017) and C1-fluidigm. Here, protein expression is studied using antibody conjugated to DNA barcodes and mRNA expression using RNA sequencing. Although these technologies have unveiled novel properties of cells which could not be deduced using a single target, they all have a major limitation. Eukaryotic cells have sub-cellular compartments inside the cell which caters to the different cellular functions. The nuclear compartment which encompasses the DNA is the site of RNA transcription and RNA splicing. The cell organelles like mitochondrion and plastids have their own semi-independent DNA machinery for RNA transcription. The cytosol compartment of the cell is where majority of the cells metabolic activities and mRNA translation into protein takes place. Since all these single cell techniques lyse the whole cell using chemicals, the compartment details and molecule localization of the target species is completely lost with crucial biological information.

Microfluidic based electrokinetics methods (SINC-seq) offers a unique solution to this problem by physically separating the cytosolic and nuclear contents via electrical lysis and isotachophoresis (ITP) (Abdelmoez et al., 2018; Kuriyama, Shintaku, & Santiago, 2015; Kuriyama, Shintaku, & Santiago, 2016a; Shintaku, Nishikii, Marshall, Kotera, & Santiago, 2014). The method leverages a hydrodynamic trap in a microfluidic channel to isolate a single cell, lyse the plasma membrane selectively via the focused electric field, separate the cytoplasmic RNA from the nucleus, and output the cytoplasmic RNA and the nucleus to the independent assays via ITP (Rogacs, Marshall, & Santiago, 2014). They demonstrated integration of the method with simultaneous RNA-seq of cytoplasmic RNA and nuclear RNA from same single cells (Abdelmoez et al., 2018). However, these approaches are currently compatible with only fresh mammalian cells and the microfluidic geometry are small to capture plant cell cluster which are bigger in size.

1.3 Perturbation of gene expression during single cell analysis

As microfluidics platforms to investigate single cells were developed, researchers found that external factors may cause gene perturbation (Saliba et al., 2014; Alles et al., 2017; Nguyen, Pervolarakis, Nee, & Kessenbrock, 2018). The main routes via which gene perturbation can be introduced into the cell samples were during sample collection, sample preparation and sample adaptation. The time point of sample collection and the time of analysis may extend anywhere between hours to days. This could lead to significant changes in the cellular activity resulting in unnatural gene perturbations of the cell sample under investigation. After sample collection, certain cells have to undergo preprocessing to make them suitable for analysis. In plant cells, this could this mean removal of cell wall network interconnecting several cells using enzymatic digestion. Removal of cell wall aids in the preparation of single protoplasts and also the elimination of the rigid cell wall barrier that enables direct access to the contents of plant cell. The perturbation

of the gene expression during the sample preparation is also critical in processing plant cells. Enzymatic digestion of cell wall introduces stress to the cell as it has been removed from its normal environment and this cause upregulation and down regulation of genes. Also, the cell samples when analyzed by microfluidic platforms have to undergo extensive adaptation steps before cell lysis namely cell loading, capturing and buffer exchange procedures. The cell loading time alone may span between 30 minutes to 2 hours affecting cell and analyte integrity. Majority of microfluidic platforms utilize fluid flow to load and capture single cell where the cells are subjected to artificial stress conditions that might induce non-biological gene perturbation. Also, the numerous cell washing and buffer exchange steps contributes to additional stress.

1.4 Strategies to reduce gene perturbation during single cell analysis

Gene perturbation in animal cells during single cell analysis procedures can be reduced by freezing the cell state before analysis. The most widely used procedure to freeze cell states is by fixing the cell. Cell fixation is the preservation of cell or tissues in a life-like state using fixatives. Fixation procedures can involve physical or chemical methods. During physical fixation the cells are subjected to heating, micro-waving and cryopreservation. Exposure to extreme temperature might affect the cell integrity and degrade the analyte species. Fixation with chemicals uses coagulating fixatives and cross-linking fixatives. Coagulating fixatives like alcohol fixates the cells by dehydration which results in loss of cell morphology, precipitation of proteins and solublization of cell membrane. Cross-linking fixatives forms covalent bonds with cell contents and retains the cell morphology. They are further classified into chemically non-cleavable cross-linkers and chemically cleavable cross-linkers. Cells fixed by using chemically non-cleavable cross-linkers like formaldehyde modifies the analyte species and make it difficult to extract RNA. Chemically cleavable cross-linkers on the other hand enables reverse cross-linking of fixation

using chemicals and facilitates easy extraction of RNA. For example cell fixation by Dithiobis(succinimidyl propionate) (DSP) can be reversed by cleaving with Dithiothreitol (DTT). Several single cell microfluidics systems have implemented fixed cell routines on their platforms (Guillaumet-Adkins et al., 2017; Alles et al., 2017; Rosenberg et al., 2018; Thomsen et al., 2016; Attar et al., 2018) and integrated with single cell RNA sequencing, but all these techniques cannot exhibit the sub-cellular fractionation of RNA from a fixed single cell.

The recent studies on single-cell analyses of plant cells typically utilize protoplasts prepared from plant cells by enzymatically digesting the cell-to-cell connection and the cell wall by incubating for 1-3 hours (Denyer et al., 2019; Jean-Baptiste et al., 2019; Macosko et al., 2015; Ryu et al., 2019; Shulse et al., 2019). Drop-seq (Shulse et al., 2019) and 10x Chromium (Denyer et al., 2019; Jean-Baptiste et al., 2019; Ryu et al., 2019) studies excluded genes potentially perturbed by the protoplasting (Birnbaum et al., 2003) in the analyses to exclude the artifact by the enzymatic reaction. To overcome this micro and nano capillary-based approaches have to developed to extract cell contents directly without perturbing the cell state (Lorenzo Tejedor et al., 2009 & 2012; Kubo et al., 2019; Torii et al., 2019). However, there are no reported technique that utilizes electric field to selectively lysing targeted cells in an intact plant tissue and extract cellular contents.

1.5 Objectives and organization of the thesis

The objective of this thesis is to develop microfluidic approaches to measure gene expression of single cells of animals and plants at reduced perturbations using elecrokinetic-based platforms.

- Animal cell: To employ a reversible crosslinking agent to fix gene expression at the time point of fixation and integrate with the electrokinetic platform.
- Plant cell: To design a microchannel for three-dimensional electrical focusing and direct extraction of cytoplasmic molecules from an intact plant cell.

The major contributions of this dissertation are as follows

- Development and modification of dithiobis(succinimidyl propionate) (DSP) based fixation of mammalian single cells and its integration with our microfluidic approach
- Demonstrating the sensitivity and reproducibility of gene expression between fresh mammalian cells and DSP fixed mammalian by single cell RNA sequencing.
- Selective permeabilization of an intact plant cell in a cluster using three-dimensional focusing of electric field.
- Extraction of charged molecules from intact plant cell using electrical lysis and ITP.

The thesis is composed of four main chapters. In chapter two, we reported the development and modification of DSP based fixation and its integration with our microfluidic approach. In chapter three, we reported an approach to extract cytoplasmic molecules from an intact plant cell in a cluster using three-dimensional focusing of the electric field. In chapter four, we summarized the contributions made in this thesis towards achieving our objective and proposed the future scope of our work.

2

Electrical lysis and RNA extraction from single cells fixed by Dithiobis(succinimidyl propionate)

2.1 Introduction

Single cell RNA sequencing (scRNA-seq) snapshots the cellular state at the time point of lysis and reverse transcription, and enables us to study complex trajectories of single-cell dynamics by profiling cells at different states. Although the state-of-the-art techniques of single-cell preparation typically completes a cell loading for 30 min in Fluidigm C1 system and for about 2 h in Drop-seq platforms, (Islam et al., 2014; Stephenson et al., 2018; Svensson, Vento-Tormo, & Teichmann, 2018) the characteristic timescales of transcription and turnover in mammalian cells are in the orders of 10 min and 10 h, (Shamir, Bar-On, Phillips, & Milo, 2016) respectively. In particular, some transcripts show rapid degradation (half-life <2 h), (Yang et al., 2003) the scRNA-seq pipeline thus potentially changes the cellular states and the integrity of RNA, and ultimately distorts the results of scRNA-seq.

Recently, several techniques of cell preservation have been integrated with scRNA-seq protocols to address the drawbacks in the preparation of single cells. Guillaumet-Adkins et al.(Guillaumet-Adkins et al., 2017) demonstrated scRNA-seq using cryopreserved cells with dimethyl sulfoxide, preserving 44% of cells as viable (86% was viable with fresh cells). Alles et

al.(Alles et al., 2017) demonstrated Drop-seq with methanol-fixed cells and reported the comparable sensitivity and repeatability with Drop-seq with fresh cells. Formaldehyde-based fixation is also compatible with scRNA-seq, (Rosenberg et al., 2018; Thomsen et al., 2016) while the protocols involve reversing crosslink at ~55˚C for several hours. Recently, Attar et al. adapted dithio-bis(succinimidyl propionate) (DSP) fixation for single-cell transcriptomic analysis using Fluidigm C1 system. (Attar et al., 2018) DSP offers a cell fixation with free of modification of nucleic acids and rapid reverse-crosslink with reducing agents such as dithiothreitol (DTT). (Espina, Liotta, & Mueller, 2013; Xiang et al., 2004)

In the current work, we have made crucial changes to the DSP fixation protocol to maintain the integrity of the plasma membrane and developed an ITP chemistry that enabled on-chip reverse crosslinking followed by electrical lysis and ITP-based RNA extraction from single fixed cells for the first time. We showed that our cell-preservation protocol using sucrose in the storage buffer significantly prolonged the integrity of the plasma membrane and reduced cell-free RNA. We demonstrated the integration of our approach with reverse transcription quantitative polymerase chain reaction (RT-qPCR) and RNA-seq and critically benchmarked the sensitivity and repeatability.

2.2 Materials and methods

2.2.1 Cell culture and staining

We maintained K562 cells in a culture media (RPMI media, Gibco Invitrogen) supplemented with 10% fetal bovine serum (ThermoFisher Scientific, 26140079) and 0.1× Penicillin-Streptomycin (Sigma) in 5% CO_2 at 37°C and passaged every three days.

To investigate the integrity of the plasma membrane, we stained the cells before fixation with a final concentration of 0.001 mg/ml calcein AM (ThermoFisher Scientific, C3099) and

8.1 µM Hoechst (ThermoFisher Scientific, H3570) incubating for 30 min at 37°C. To visualize the RNA extraction from single fixed cells, we stained RNA with 1.25× SYBR Green II (TaKaRa, 5771A) incubating for 30 min at 37°C before the fixation.

2.2.2 Protocol of fixation with DSP

We fixed the K562 cells using reversible cross-linker DSP (ThermoFisher Scientific, 22585) with a modification from a protocol proposed by Attar et al.(Attar et al., 2018) To prolong the integrity of the plasma membrane of DSP-fixed cells, we supplemented 9.3% sucrose (Sigma, S0389) in the storage buffer, which consisted of phosphate buffered saline (PBS) and 20 mM Tris-HCl (pH 7.5). Our protocol started with fresh 200,000 cells and washed twice with PBS with centrifugations at 94 × g for 3 min. We then fixed the cells in 200 µl of a freshly prepared DSP buffer (1× DSP in 1× PBS) incubating for 30 min at room temperature. We quenched the cross-link reaction by adding 4.1 µl of 1 M Tris-HCl (pH 7.5). We transferred 150 µl of the fixed cells to a new microfuge tube, added 27.5 µl of 60% sucrose in a PBS containing 20 mM Tris-HCl (pH 7.5), and stored in 4°C until further processing. We stored the remaining fixed cells suspended in a PBS containing 20 mM Tris-HCl (pH 7.5) as control samples.

2.2.3 Alternative fixation protocols

To benchmark our protocol of fixation, we prepared cells fixed with methanol (Wako, 134-11821) and ethanol (Wako, 052-07221). (Alles et al., 2017; Wu et al., 2001) To fix cells with methanol, we centrifuged 1-4 $\times 10^6$ cells at 94 × g for 3 min at 4°C and re-suspended in 200 µl of ice-cold PBS. We then added 800 µl of methanol (pre-chilled at -20°C) drop-by-drop with gentle vortexing. We incubated the cells on ice for 15 min. To prepare the cells for ITP protocol, we centrifuged the methanol-fixed cells at 94 × g for 3 min and re-suspended the cells in 1 ml of PBS containing 0.01% of bovine serum albumin for storage. To fix cells with ethanol, we washed cells

with PBS by centrifuging at 94 × g for 3 min and suspended in 0.5 ml of PBS. We added 5 ml of 70% ethanol (pre-chilled at -20°C) and incubated them on ice for 1 h. We then exchanged the solution with 1 ml of the culture media for storing.

2.2.4 ITP buffers

The leading electrolytes (LE) were 50 mM Tris and 25 mM HCl containing 0.4% poly(vinylpyrrolidone) (PVP) (calculated pH of 8.1). The trailing electrolytes (TE) were 50 mM Tris, 25 mM HEPES, 0.4% PVP (calculated pH of 8.3) and 5 mM DTT for on-chip reverse crosslinking of DSP-fixation. We used TE buffers *sans* DTT for control experiments with fresh cells and fixed cells by ethanol and methanol. We included PVP to suppress electroosmotic flow.

2.2.5 Microfluidic method of RNA extraction from fixed single cells with electrical lyses & ITP

We fabricated polydimethylsiloxane (PDMS, Sylgrad 184, Dow Corning) microchannel superstructures with soft-lithography and bonded to a glass substrate.

We washed and preconditioned the microchannel by filling the inlet and outlet well with wash buffers and applying vacuum to the waste well. Our washing sequences were as follows: 1 M NaOH for 1 min, 1 M HCl for 1 min and deionized (DI) water for 1 min. All washing buffers contained 0.1% Triton X-100 to prevent bubble trapping in the hydrophobic channel. Following this, we loaded 10 µl of LE and TE to the outlet and inlet wells respectively and applied vacuum to the waste well to fill the microchannel with LE and TE buffer. We removed the LE and TE buffers from the wells and filled the outlet and inlet wells with 8.5 µl of LE and TE buffers, respectively. We then loaded 1 µl of cell suspension containing a single fixed cell into the inlet well and introduced it into the microchannel via the pressure driven flow. After visually confirming the captured single cell at the hydrodynamic trap, we dispensed 3.2 µl of TE buffer in the waste well to suppress the pressure driven flow. We placed 300 µm diameter platinum electrodes into

the wells and applied -150 V, -170 V and 0 V to the electrodes at the inlet, waste and outlet wells, respectively. The applied DC voltage formed a focused electrical field at the hydrodynamic trap and lysed the plasma membrane within 1 s. The suitable interface of ITP buffers at the T junction enabled fast focusing of RNA into the ITP-zone at TE-to-LE interface. After 80 s, we changed the voltages at the inlet and waste wells to -350 V and -510 V, respectively, to accelerate the migration of the ITP zone. The ITP delivered the RNA to the output well in about 100 s to 120 s as the current signal plateaued, while the nucleus was physically retained at the hydrodynamic trap. We switched off the voltages at 240 s and dispensed 10 µl of LE in the waste well to prevent pressure driven flow from the outlet well into the microchannel. We mixed the solution in the outlet well by pipetting and transferred it to a fresh microfuge tube. We removed the TE solution from the inlet well and washed the inlet thoroughly with 10 µl of LE buffer. We added 4 µl LE buffer to inlet well and applied pressure from the waste well to push the nucleus into the inlet well. After visually confirming the presence of the nucleus in the inlet well, we transferred 4 µl of the solution including the nucleus to a fresh microfuge tube.

2.2.6 Quantification of extracted RNA with RT-qPCR

We quantified the extracted RNA and RNA retained in the nucleus with RT-qPCR. We targeted glyceraldehyde 3-phosphate dehydrogenase (*GAPDH*). We used TaqMan Gene Expression Assays (Hs02758991_g1) and RNA-to-Ct 1-Step Kit (Thermo Fisher Scientific, 4392938). We calculated the percent fraction of extracted RNA, *f*, as

$$f = \left(\frac{2^{-Ct_{cyt}}}{2^{-Ct_{cyt}}+2^{-Ct_{nuc}}}\right) \times 100, \quad (1)$$

where Ct_{cyt} and Ct_{nuc} are *Ct* values with ITP-extracted RNA and with a nucleus, respectively.

2.2.7 Library preparation and RNA seq analysis

We synthesized cDNA respectively with the extracted RNA and nucleus using Smart-Seq2 protocol (Clontech, 634891) with 18 PCR cycles following the manufacturer's manual. We spiked 1 µl of ERCC diluted 10^7 fold in UltraPure DNase-/RNase-free deionized (DI) water (Life Technologies) to the extracted RNA and nucleus before the protocol. We assessed the yield and quality of the purified cDNA using Qubit (ThermoFisher Scientific, Q33222) and qPCR targeting *GAPDH* and gamma-globin genes (*HBG*, Hs00361131_g1).

We performed the tagmentation with 200 pg of cDNA using NEXTRA XT DNA sample prep kit (Illumina, FC-131-1096) according to the manufacturer's protocol, except we eluted the library in 24 µl of the elution buffer. We pooled the 16 libraries and carried out sequencing using MiSeq (MiSeq Reagent Kit v3, Illumina) with 75 base paired-end reads. Using STAR (version 2.5.3a) with ENCODE options, (Dobin et al., 2013) we mapped the reads to the human reference genome (GRCh 38.86) and calculated the expression estimates in TPM using RNA-seq by expectation maximization (RSEM version 1.3.0). (Li & Dewey, 2011)

To benchmark our protocol, we compared the RNA-seq data of single fixed cells with those of single fresh cells. In this comparison, we used data of single fresh cells by Abdelmoez et al.(Abdelmoez et al., 2018) down-sampling the raw reads to be the same average sequencing depth using Seqtk (https://github.com/lh3/seqtk/).

2.2.8 Calculations of log_2 fold change

To benchmark the efficiency of the extraction, we compared the gene expressions of extracted RNA between fresh cells and DSP-fixed cells. We used $\log_2$ fold change, FC_i, comparing DSP-fixed cells versus fresh cells as

$$Log_2FC_i = mean\left(Log_2\left(TPM_{FX,i}+1\right)\right) - mean\left(Log_2\left(TPM_{FR,i}+1\right)\right), \quad (2)$$

where $TPM_{FX,i}$ and $TPM_{FR,i}$ are respectively TPM values of gene i with a DSP-fixed cell and a fresh cell. We used FC_i in our analysis only when the differential gene test function of Monocle2 resulted in successful statistics. (Trapnell et al., 2014)

2.3 Results and discussion

2.3.1 Electrical lysis and ITP-based RNA extraction from fixed single cells

Our new ITP chemistry uniquely enables our microfluidic method of electrical lysis and ITP-aided RNA extraction from single DSP-fixed cells (Fig. 2.1). In the microfluidic system, we isolated a fixed cell at the hydrodynamic trap (Fig. 2.1D), reverse-crosslinked by on-chip reaction with DTT in the TE buffer (Fig. 2.3), lysed the plasma membrane selectively (Fig. 2.1E), and extracted cytoplasmic RNA (Fig. 2.1F). We exploited the focusing effect of the electrical field at the trap to reduce the applied voltages, selectively lyse the plasma membrane of the fixed cell, and separate the nucleus from cytoplasmic RNA by retaining the nucleus at the trap. The microfluidic method completed in less than 5 min and outputted the extracted RNA and nucleus respectively to independent off-chip analyses. We also show dynamics of lysis and extraction of calcein molecules from single fixed cells with a supplementary movie.

To benchmark our microfluidic method of RNA extraction from fixed cells, we quantified *GAPDH* by RT-qPCR in the extracted RNA and retained RNA (nucleus), as shown in Figure 2.2A. We observed negligible significance in the comparison of fixed (n = 12) versus fresh cells (n = 7) with both extracted RNA ($p = 0.21$) and retained RNA ($p = 0.92$). We further benchmarked the DSP fixation comparing to the alternative fixation protocols with methanol (Alles et al., 2017) and ethanol (Wu et al., 2001). Among the three fixation protocols, the DSP fixation presented the best performance with the highest fraction of extracted RNA (Figure 2.2B. See also raw Ct values in Figure 2.4). These results demonstrated the compatibility of the DSP fixation with our microfluidic

approach.

We note that the methanol fixation, which was compatible with Drop-seq, (Alles et al., 2017) was able to retain RNA in the fixed cell (See the estimated equivalent Ct values with the total RNA in Fig. 2.4), but it was incompatible with our electrical lysis and ITP-based RNA extraction. Our approach, which extracts charged molecules, requires the hydrated state of the molecules to exert the Coulombic force on them. We thus hypothesize that this significantly low extraction efficiency of methanol-fixed cells is due to dehydration in the cell body.

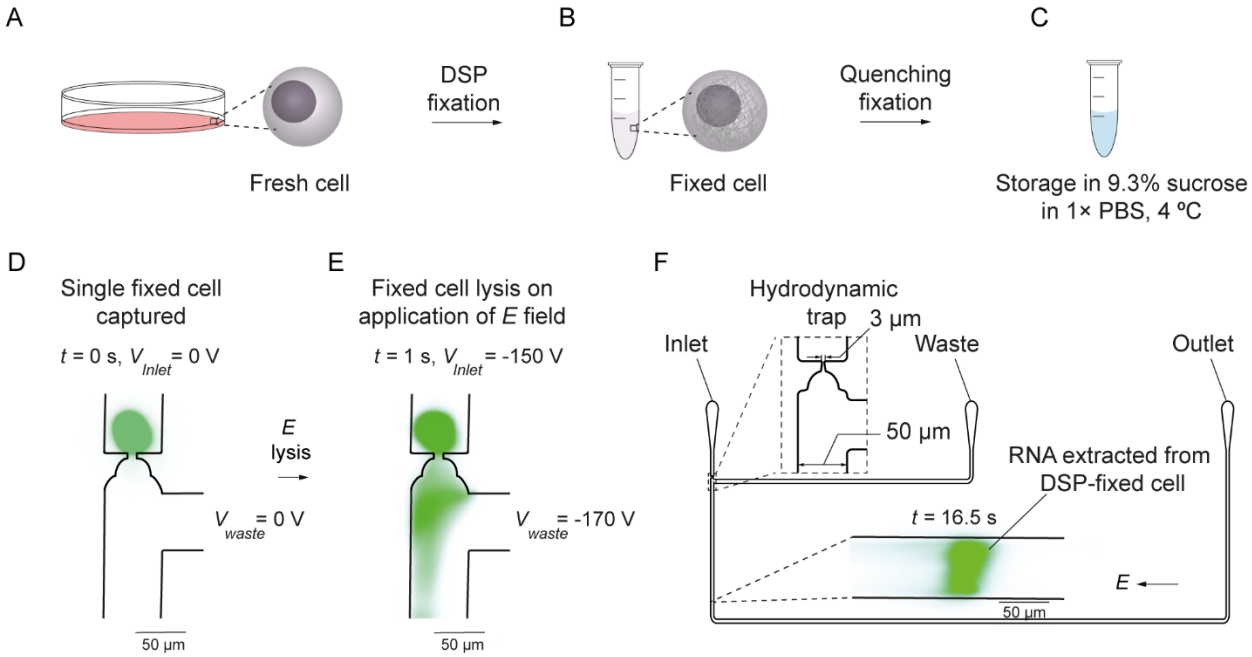

Figure 2.1 Overview of cell fixation protocol with DSP and extraction of cytoplasmic RNA from fixed single cells by electrical lysis and ITP-aided extraction. (A-C) Workflow of DSP fixation and storage in PBS including 9.3% sucrose. (D, E) Typical fluorescence images (false color, SYBR Green II) of a single fixed cell at a hydrodynamic trap and extraction of RNA via electrical lysis and ITP. (F) Overview of the microfluidic system and focused RNA at ITP-zone

To optimize the DTT concentration, we performed our microfluidic protocol with various concentrations of DTT in the TE buffer, ranging from 5 mM to 100 mM. We observed that the ITP dynamics became less repeatable at high DTT concentrations. We show examples of the measured current profiles at 5 mM DTT and 100 mM DTT in Fig. 2.5, indicating the larger variation in the current at 100 mM. We also observed no apparent improvement in the extraction of RNA via RT-qPCR with high DTT concentrations. We thus performed our experiments at 5 mM of DTT.

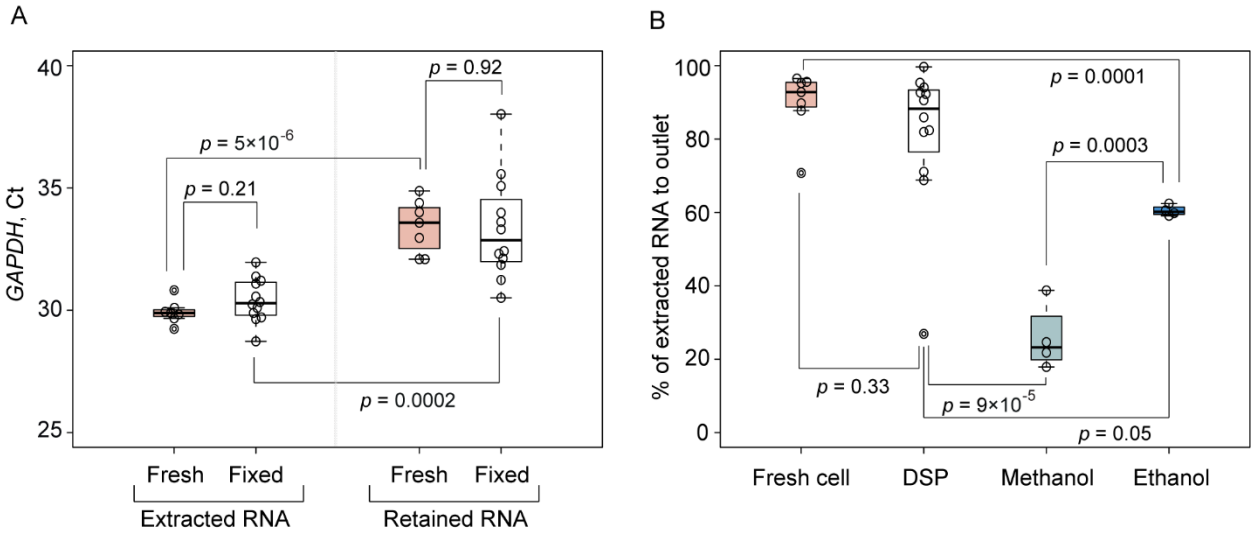

Figure 2.2 Extraction efficiency of cytoplasmic RNA from fixed cells via electrical lysis and ITP-based extraction. (A) Comparison of Ct values of extracted RNA and retained RNA of fresh cells and DSP-fixed cells. (B) Comparison of DSP-fixation to methanol and ethanol fixation protocols with % fraction of extracted RNA defined by Eq. (1)

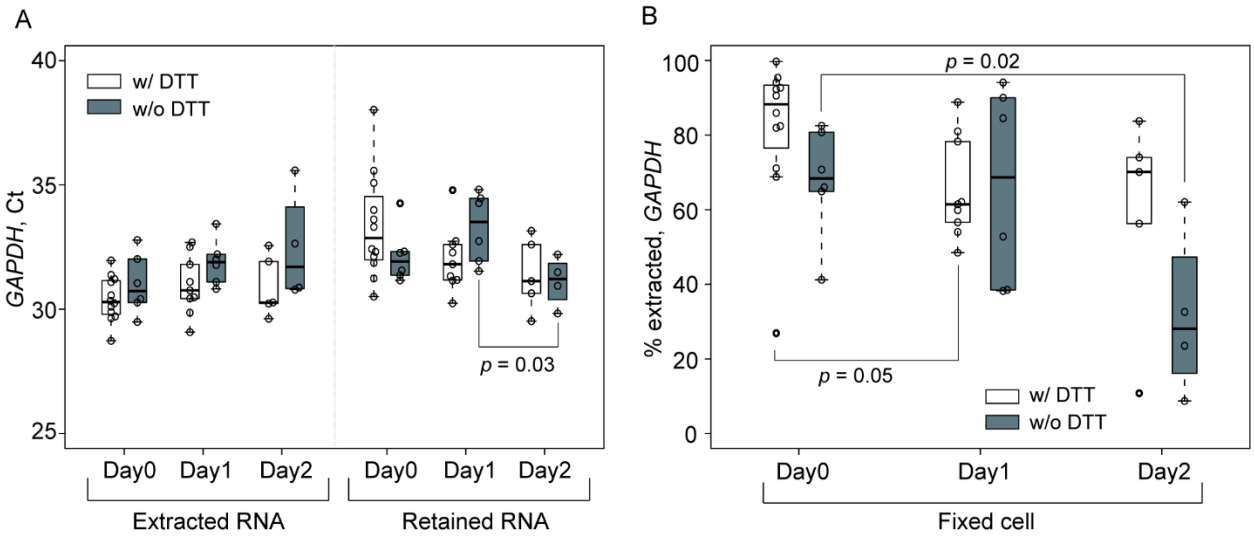

Figure 2.3 On-chip reverse crosslink with DTT. (A) Raw Ct data taken with extracted RNA and retained RNA comparing with versus without DTT in the TE buffer. (B) % fraction of extracted RNA with and without DTT in the TE buffer

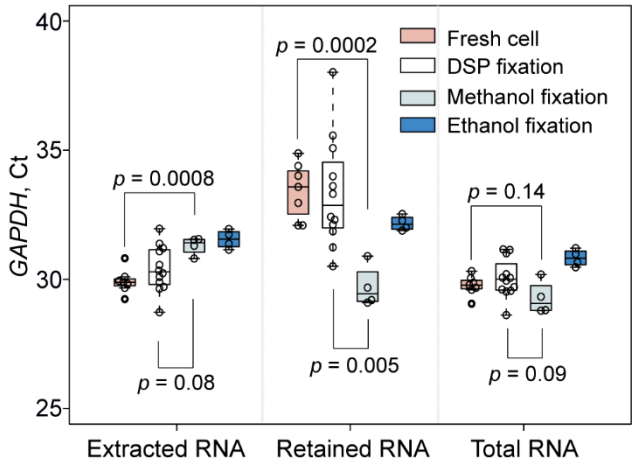

Figure 2.4 Raw Ct values for estimating % fraction of extracted RNA from cells with various fixation protocols. Values of total RNA were equivalent Ct values that were estimated by taking the summation of the extracted RNA and retained RNA

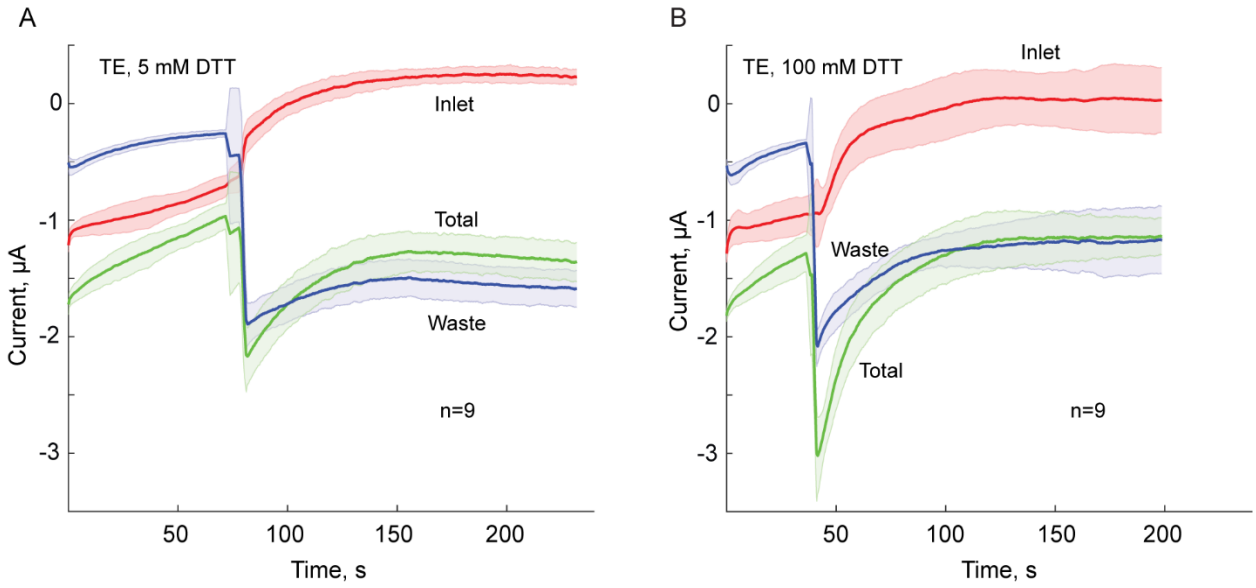

Figure 2.5 Examples of measured current during ITP-based extraction of RNA at two DTT concentrations of A) 5 mM and B) 100 mM. Lines and envelopes show mean and standard deviation, respectively

2.3.2 Sucrose prolongs cell membrane integrity of DSP-fixed cells

In addition to coupling the DSP-fixation with our microfluidic method, we modified the storage buffer from the protocol proposed by Attar et al. (Attar et al., 2018) to reduce the cell-free RNA by supplementing 9.3% sucrose to the storage buffer. The suppression of cell-free RNA is crucial in scRNA-seq protocols to prevent the cross-contamination. (Gierahn et al., 2017) Sucrose is known as a protein stabilizer and is used in tissue preservations, which use ~10% and ~30% sucrose solutions. (Prestrelski, Tedeschi, Arakawa, & Carpenter, 1993; Rye, Saper, & Wainer, 1984) To avoid too much hypertonic condition, we designed the sucrose concentration at 9.3% and determined its applicability by observing the integrity of the plasma membranes. We found that the sucrose significantly prolonged the integrity of plasma membranes (Fig. 2.6A-C, Fig. 2.7 & 2.8) and thus reduced the cell-free RNA especially in the aged samples (Fig. 2.6D). See also Fig. 2.9 for raw Ct values). Further, the preserved calcein molecules (Fig. 2.6A-C), which were

free from the DSP crosslinking, indicated that the storage buffer enabled the DSP-fixed cells to retain the molecules with no primary amines. This indicates that the modified protocol is potentially useful for studying small molecules including metabolites of single cells, while it is beyond our focus.

We also explored the efficiency of RNA extraction comparing with and without sucrose in the storage buffer as shown in Fig. 2.10. The sucrose increased amount of extracted RNA with aged samples (Day1 and Day2) as shown in Fig. 2.10A and contributed to improving the extraction efficiency slightly (Fig. 2.10B). However, we found that the fraction of extracted RNA gradually decreased with increasing storing time in comparison to the fresh cells. We hypothesize that the decrease in the extraction efficiency is not mainly due to the degradation of RNA as we see no apparent change in the Ct values with whole single cells (Fig. 2.11), while the decrease may be due to further crosslink or dehydration of molecules during the storage. We hope to address this low efficiency in the future work by further optimizing the protocol parameters including quenching the crosslink, applied voltages, the concentration of DTT, and concentration of sucrose.

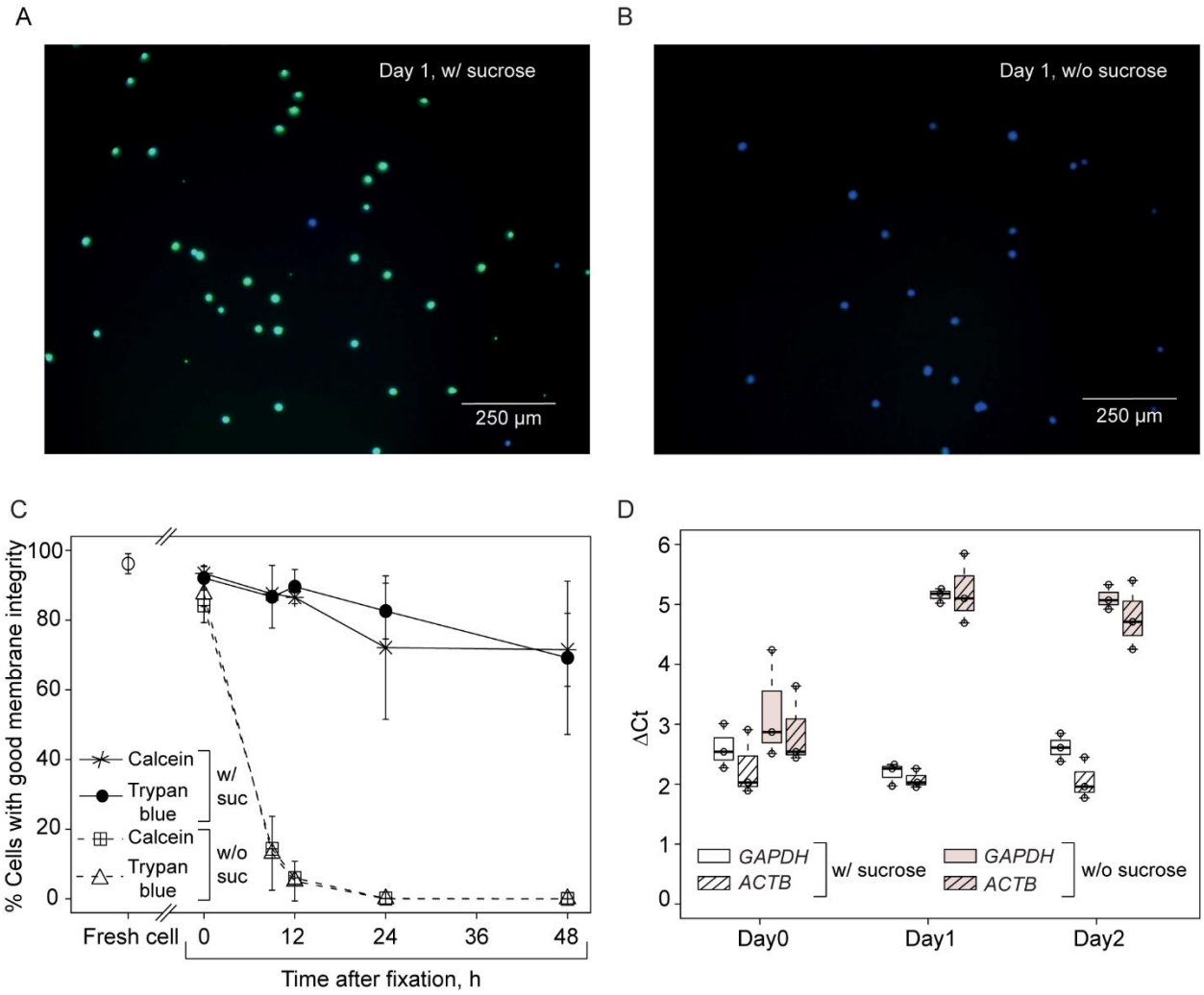

Figure 2.6 Effect of sucrose in the storage buffer on the membrane integrity and cell-free RNA. (A, B) False color images of calcein (green) and Hoechst (blue) of fixed K562 cells on day 1 stored in PBS with and without sucrose, respectively. (C) The fraction of cells with good membrane integrity assessed with calcein and trypan blue. (D) Cell-free RNA level ($\Delta Ct = Ct_{fresh} - Ct$) in the storage buffers with and without sucrose.

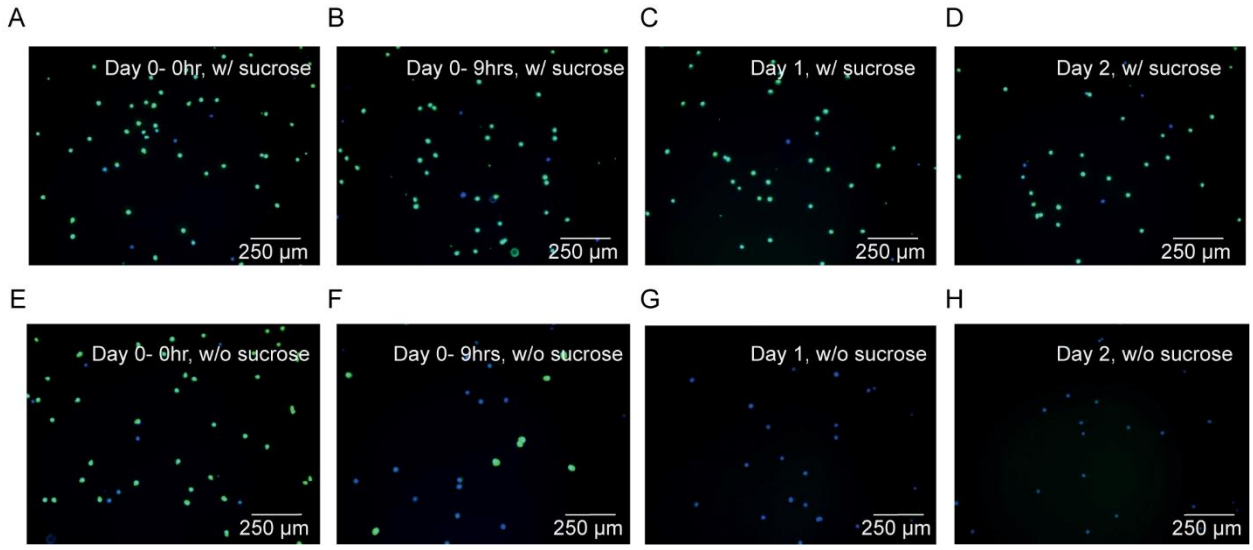

Figure 2.7 False color images of calcein (green) and Hoechst (blue) fluorescence from fixed cells stored in PBS (A-D) with and (E-H) without sucrose at four-time points since the fixation.

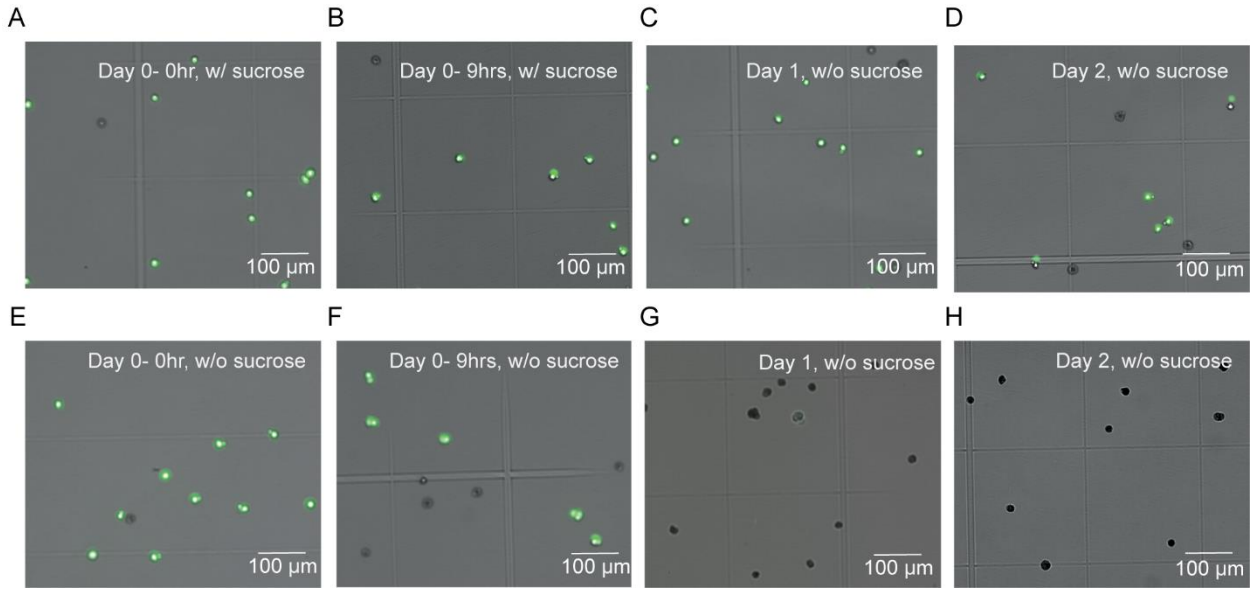

Figure 2.8 False color images of calcein fluorescence(green) and trypan blue (dark spots) from fixed cells stored in PBS (A-D) with and (E-H) without sucrose at four-time points since the fixation.

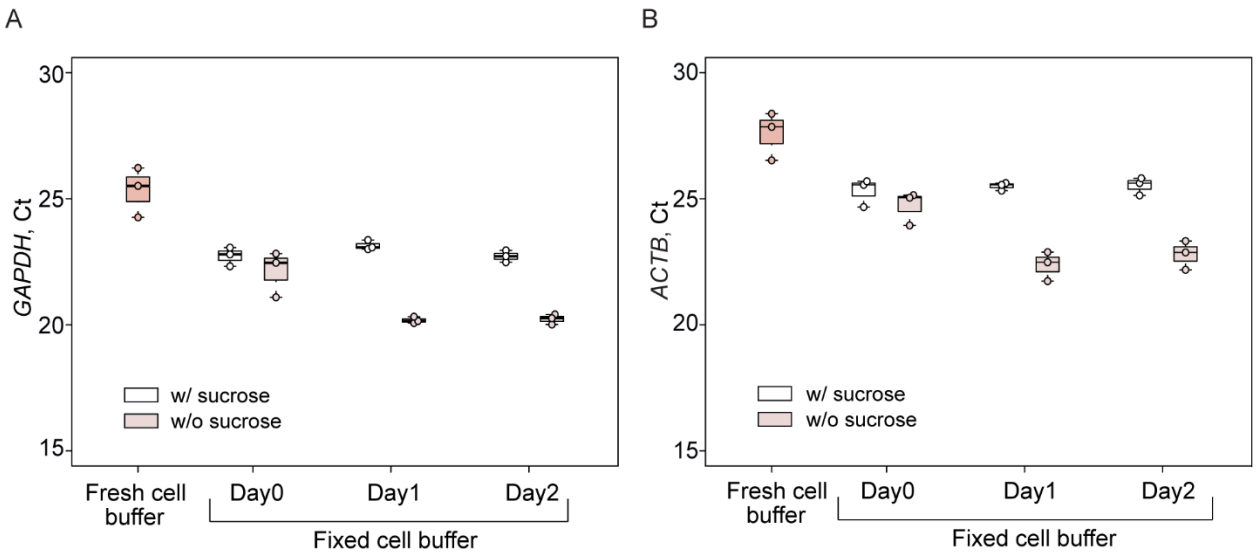

Figure 2.9 Raw Ct values in cell-free RNA experiments targeting (a) GAPDH and (b) ACTB, respectively

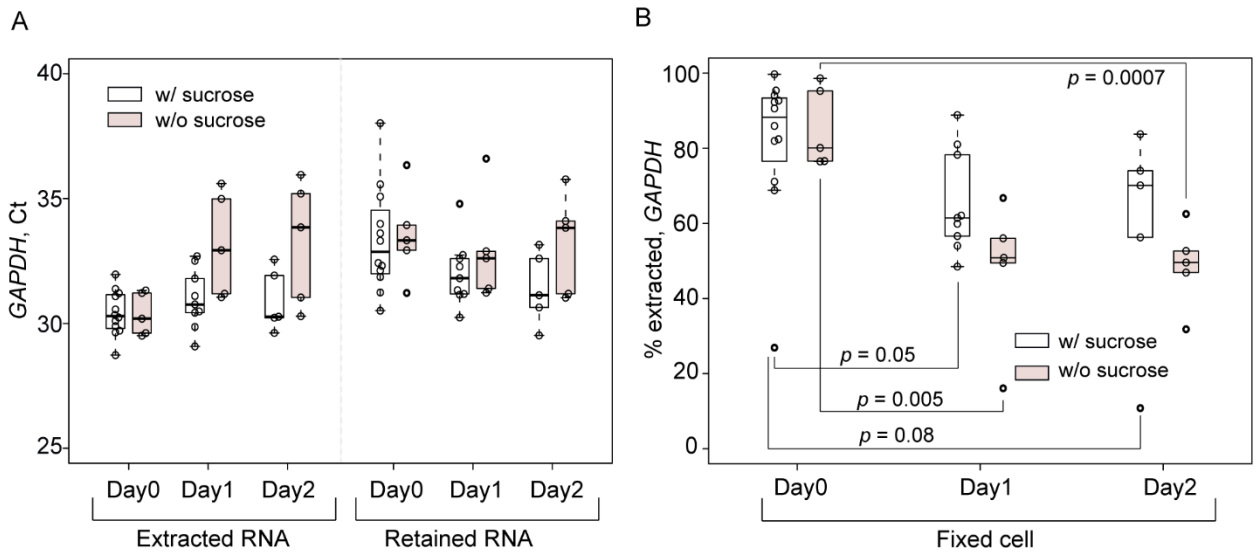

Figure 2.10 Raw Ct values for estimating % fraction of extracted RNA. Percent fraction of extracted RNA estimated with GAPDH gene

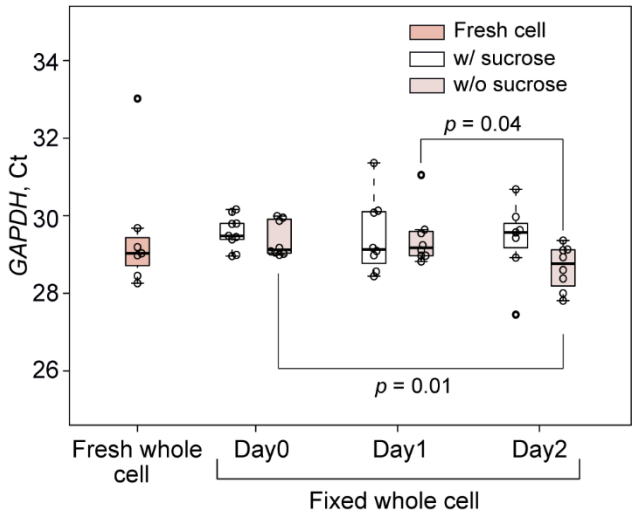

Figure 2.11 Effects of DSP fixation and aging on Ct values assayed with single cells targeting GAPDH

2.3.3 Compatibility with RNA sequencing

To explore the compatibility of our method with high-throughput RNA sequencing, we carried out experiments with eight DSP-fixed cells (Day 0), constructed RNA-seq libraries with both extracted RNA and retained RNA, and performed RNA-seq. Of 16 libraries (extracted and retained fractions) created with the eight DSP-fixed cells, all passed the quality control before the sequencing and resulted in 3.2±2.0 M paired-end reads per sample; and 94±2% of reads was aligned on the reference genome. We note that to balance the cost and sensitivity we designed the sequencing depth to be shallower than that by Abdelmoez et al., (Abdelmoez et al., 2018) but more than ~2 M paired-end reads, at which we observed a saturation in the gene detection.

To evaluate the extraction efficiency of our method, we compared the gene expression of extracted RNA between DSP-fixed cells and fresh cells. Figures 2.12A and B show the number of detected genes comparing fixed versus fresh cells and the coefficients of a paired correlation, respectively. The DSP-fixed cells displayed a smaller number of detected genes and reduced repeatability, consistent with the yield of cDNAs with respective samples (Fig. 2.14). To test whether the transcript length affected the extraction of RNA, we divided the short (<1kb) versus the long transcripts (>1kb) and compared the mean $\log_2$ fold change (Fig. 2.15A). The histogram of long transcripts particularly showed reduced expression in the extracted RNA from the fixed cells, implying the length bias existed in the extraction. Although the average log2 fold change of short transcripts were -0.24, which was 85% relative to the fresh cells, that of long transcripts was -1.12 meaning 46% relative to fresh cells. Interestingly, despite these remaining problems, the averaged gene expression of DSP-fixed cells was highly consistent with those of fresh cells with r=0.91 of Pearson correlation (Fig. 2.15B).

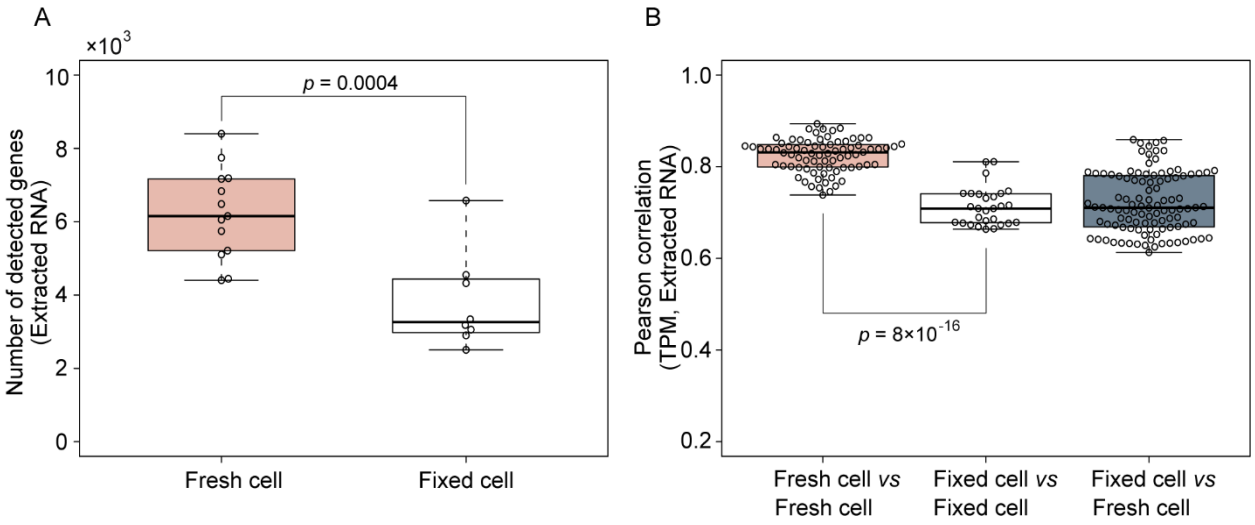

Figure 2.12 (A) Comparison of a number of detected genes with extracted RNA from DSP-fixed cells versus fresh cells. (B) A paired correlation computed with gene expressions of extracted RNA

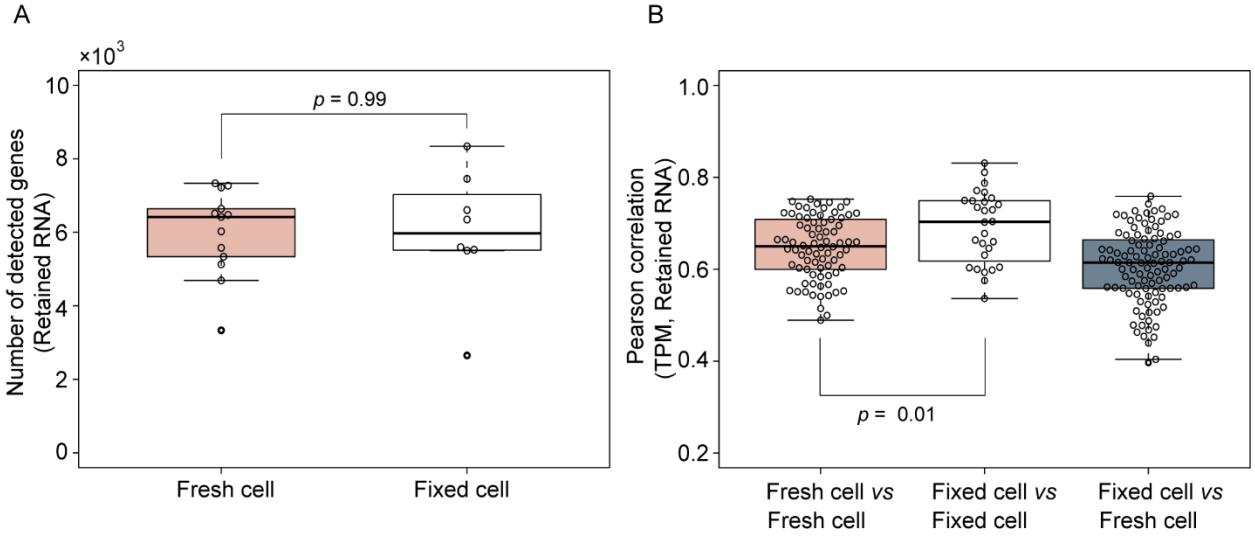

Figure 2.13 A) Comparison of numbers of detected genes with retained RNA from DSP-fixed cells versus fresh cells. B) A paired correlation computed with gene expressions of retained RNA

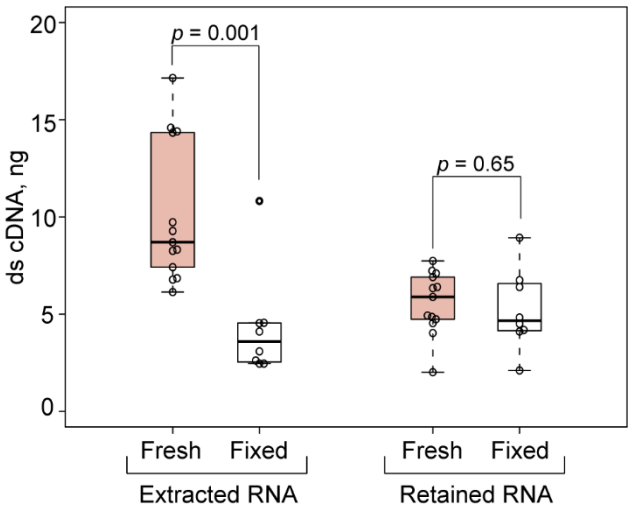

Figure 2.14 Comparison of cDNA yield with extracted RNA and retained RNA between fixed and fresh cells

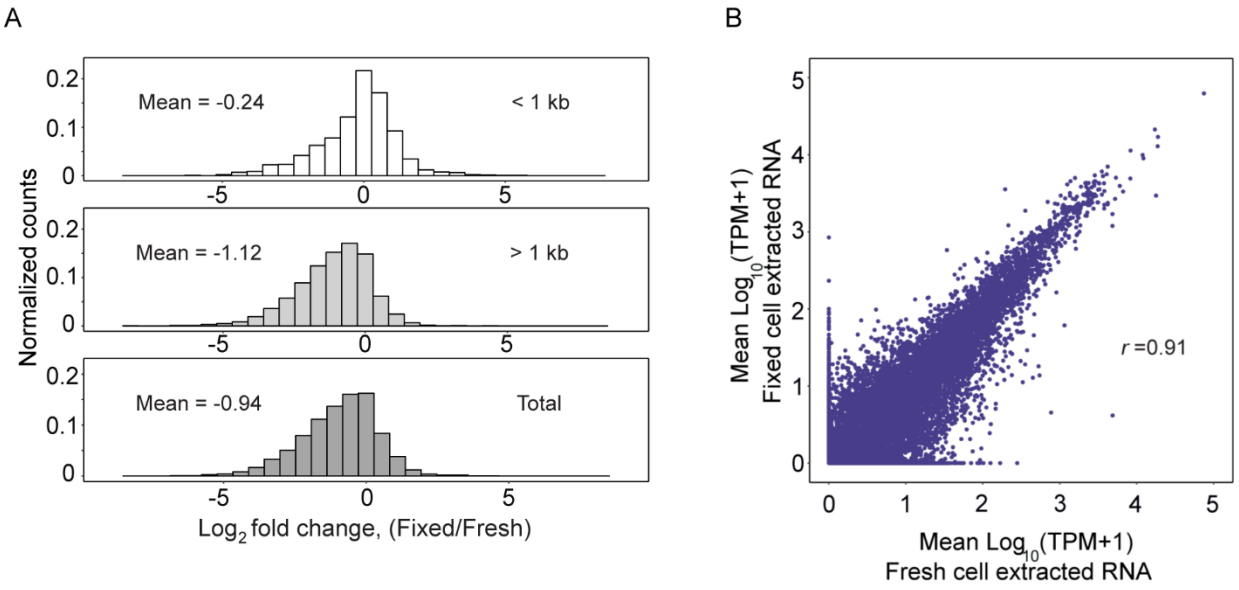

Figure 2.15 (A) Effect of length of transcripts on extraction efficiency assessed with Log2 fold change of fixed versus fresh cells with short transcripts (<1 kb, top panel) and long ones (>1 kb, middle panel). Overall Log2 fold change (bottom panel). (B) Comparison of gene expression patterns of extracted RNA from DSP-fixed cells versus fresh cells

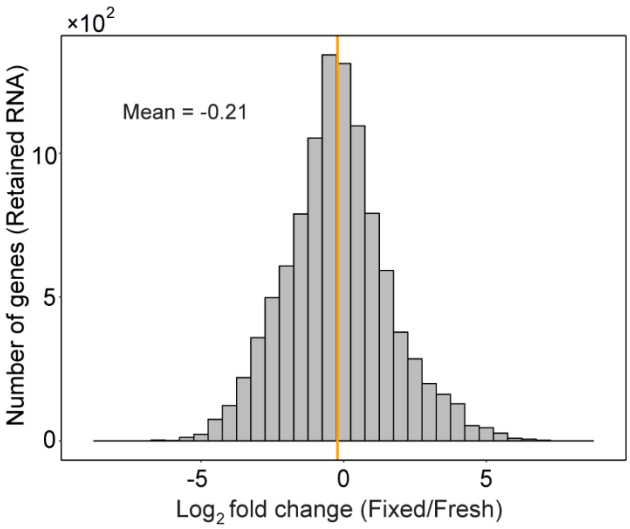

Figure 2.16 Log2 fold change of gene expression of retained RNA comparing DSP-fixed cells versus fresh cells

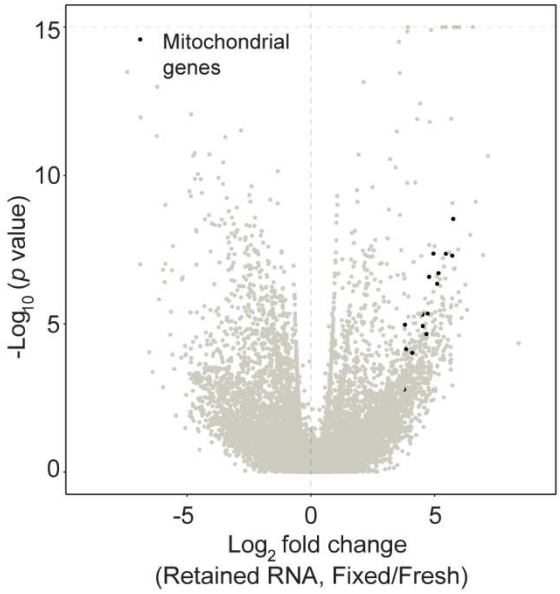

Figure 2.17 Differentially expressed genes (DEG) of retained RNA comparing fixed versus fresh. We computed p values with the negative binomial model of Monocle2 and expected counts computed with RSEM. We cut off -Log$_{10}$p higher than 15 and then plotted them at -Log$_{10}$p =15

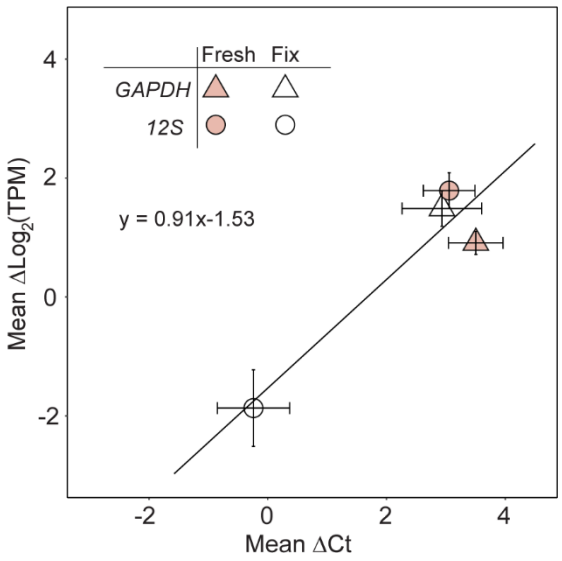

Figure 2.18 Correlation plot between mean $\Delta Ct = (Ct_{nuc} - Ct_{cyt})$ from RT-qPCR and mean $\Delta Log_2(TPM) = (Log_2(TPM_{cyt}) - Log_2(TPM_{nuc}))$ from scRNA sequencing

To elucidate the source of the reduced sensitivity and repeatability in RNA-seq with the extracted RNA, we next assessed the retained RNA of the fixed cells for a number of detected genes and correlation of gene expression. Figures 2.13 A and B show that the retained RNA of DSP-fixed cells exhibited comparable sensitivity and slightly better repeatability to those of fresh cells. Additionally, we performed differentially expressed gene (DEG) analysis (Li & Dewey, 2011) with retained RNA comparing fixed versus fresh cells (Fig. 2.12 & 2.16). We observed a mean $\log_2$ fold change close to zero (Fig. 2.16) indicating similar gene expression profiles in the retained RNAs and consistent with the yields of cDNA (Fig. 2.14). However, we also observed a significant over expression of the mitochondrial genes (Fig. 2.17), which were useful biomarkers to evaluate fractionation. (Abdelmoez et al., 2018) This implied that the retained RNA of DSP-fixed cells had increased contamination from cytoplasmic RNA compared to that of fresh cells. We thus hypothesize that the reduced sensitivity and repeatability observed with the extracted RNA are due to both the reduced extraction from the DSP-fixed cell and the insufficient transport of cytoplasmic RNA via ITP to the outlet. We hope to address these issues by further optimizing the protocol

parameters in the future.

To effectively explore various conditions, we characterized our microfluidic method using RT-qPCR targeting *GAPDH*. RT-qPCR was sensitive and reproducible enough to characterize the overall performance of the protocols. We validated our approach by measuring the ratio of extracted versus retained RNA with RT-qPCR in comparison to RNA-seq on Day 0 samples as shown in Fig. 2.18, which showed the consistency with a slope of 0.91 between them. We also note that our protocol of RNA-seq is more labile than RT-qPCR as RNA-seq primes the reverse transcription with poly (A) of mRNA while RT-qPCR does with a specific primer targeting a small locus. We thus hypothesize that RT-qPCR potentially overpredicts the yield of the RNA-seq protocol when evaluating aged samples.

In summary, the new ITP chemistry enabled on-chip reverse crosslinking and coupled extraction of RNA from DSP-fixed cells via electrical lyses of plasma membranes with ITP-based nucleic acids extraction. We here show the compatibility of the extracted RNA and retained RNA with high throughput RNA-seq. Despite the reduced sensitivity and repeatability with RNA-seq, the method was reproducible, where we succeeded in preparing all the sequencing samples and consistently detected more than 2,000 genes per sample. We also found that RNA-seq with the extracted RNA from DSP-fixed cells could provide a similar pattern of gene expression to that from fresh cells.

2.4 Summary

We reported a new ITP chemistry that uniquely enabled electrical lysis and extraction of RNA from single DSP-fixed cells. We demonstrated integrations of our method with off-chip RT-qPCR and RNA-seq, and discussed the efficiency of RNA extraction. We showed the compatibility of DSP-fixation with our microfluidic approach comparing to fresh cells, methanol fixation, and

ethanol fixation. We showed that the DSP-fixation offered the highest efficiency of RNA extraction compared to the other two fixation protocols. Gene expression analyses with extracted RNA from single DSP-fixed cell displayed reduced repeatability and sensitivity compared to those with fresh cells, yet the averaged gene expression pattern was highly consistent with those of fresh cells. Unlike experiments with single fresh cells, cell fixation via DSP separates the sample collection from the downstream processing and enables coupling with the electrical lyses and extraction of RNA from fixed cells. Therefore, the method would allow us to design complex studies. In addition to RNA-seq with both fractions as demonstrated in this study, the method may be easily extended to parallel analyses of genomic DNA versus RNA from the same single fixed cells. (Kuriyama et al., 2015) We hope to demonstrate such additional applications and explore the cascade from the epigenetic modification of genomic DNA to transcriptomic events in the future.

3

Targeted permeablization of cell wall and extraction of charged molecules from single cells in intact clusters using focused electric field

3.1 Introduction

Cellular heterogeneity in plants has largely been unexplored using single-cell approaches. This is partly due to the technical challenges that plant cells impose. To begin with, it is difficult to isolate an intact single plant cell from the three-dimensionally organized tissues because of the cell-cell connection and the cell wall, which is a layered structure mainly consisting of cellulose microfibrils and surrounding the plasma membranes of plant cells. Furthermore, the cell wall act as a physical barrier to extract cellular contents.

Lately, studies on single-cell analyses of plant cells employs protoplasts prepared from plant cells by enzymatically digesting the cell-to-cell connection and the cell wall and incubating for 1-3 hours (Denyer et al., 2019; Jean-Baptiste et al., 2019; Macosko et al., 2015; Ryu et al., 2019; Shulse et al., 2019). Protoplasts are immediately adaptable with microfluidic platforms, such as Drop-seq (Shulse et al., 2019) and 10x Chromium (Denyer et al., 2019; Jean-Baptiste et al., 2019; Ryu et al., 2019), that were developed for single cells of animals, and yields high-throughput gene expression information from tens and thousands of single protoplast. These studies excluded

genes potentially perturbed by the protoplasting (Birnbaum et al., 2003) in the analyses to exclude the artifact by the enzymatic reaction.

On the other hand, micro/nano capillary-based approaches are ideal to sample cellular contents for measuring the gene expression or metabolic signature from a living plant cell without perturbing the cellular state of the interest and further with preserving the viability of non-targeted cells in the tissue. Tejedor et al. (Lorenzo Tejedor, Mizuno, Tsuyama, Harada, & Masujima, 2009, 2012) demonstrated sampling of cellular contents from a single plant cell by inserting a nanoelectrospray tip (a glass capillary with a tip of 1 μm in the inner diameter) to a targeted cell and performed the mass spectrometry on the metabolites. Kubo et al. (Kubo et al., 2019; Torii et al., 2019) proposed a microcapillary-based approach that mechanically disrupted the cell wall and aspirated the cellular contents from a targeted cell in plant tissue. This approach enabled gene expression analysis of single plant cells without enzymatic reaction and offered to infer the spatial influence of the cell on the transcriptomic profile obtaining the positional information of the targeted plant cells. Nashimoto et al. (Nashimoto, Echigo, Ino, & Shiku, 2019) demonstrated transcriptional analysis of living single cells in an intact spheroid of mammalian cells with a nanopipette extracting cytosol via electrochemical syringe (Ito et al., 2017; Nashimoto et al., 2016). Capillary-based approaches can also be coupled with the electric field-based lysis and extraction (Han et al., 2003; McClain et al., 2003). However, to our knowledge, there is no report on an electric field-based technique selectively lysing targeted cells in intact plant tissue and extracting the cellular contents for the transcriptomic analyses.

We reported electric field-based lysis and extraction of cytoplasmic RNA molecules from a single mammalian cell with microfluidic approaches (Abdelmoez et al., 2018; Abdelmoez et al., 2020; Khnouf et al., 2018; Kuriyama, Shintaku, & Santiago, 2015; Kuriyama,

Shintaku, & Santiago, 2016b; Subramanian Parimalam et al., 2018). Our approach leveraged a hydrodynamic trap that focused the electric field for lysing the plasma membrane selectively and extracting cytoplasmic RNA from the lysed cell coupling with isotachophoresis (ITP)-aided nucleic acids extraction (Rogacs, Marshall, & Santiago, 2014). Our approach offered fractionating the cytoplasmic RNA vs. nucleus and enabled multi-omics analyses of cytoplasmic vs. nuclear RNA (Abdelmoez et al., 2018) or cytoplasmic RNA vs. genomic DNA (Kuriyama et al., 2015; Shintaku et al., 2014) integrating with high-throughput sequencing (Abdelmoez et al., 2018; Khnouf et al., 2018).

In the current work, we present a new microfluidic approach that enables the electric field-based permeabilization of cell walls and the electrophoretic extraction of cytosolic molecules from targeted cells in a cluster of intact plant cells via focused electric field coupling with ITP-aided extraction (Fig. 3.1) The approach completes the entire steps starting from permeabilizing the cell wall, extracting the cytosolic molecules, and outputting them to the outlet reservoir for off-chip analyses with controlling the electric field via end-channel electrodes inserted in the terminal reservoirs. To overcome the barrier due to the cell wall, we designed a three-dimensional microchannel enabling one-order of magnitude stronger focusing on the electric field. We also employed an intense pulsed electric field that selectively permeabilized the cell walls of a few targeted cells in intact plant clusters. We demonstrated the integration of our approach with the on-chip fluorescence measurement of the extracted molecules and off-chip reverse transcription-quantitative polymerase chain reaction (RT-qPCR) targeting mRNA in the extracted molecules. The results show that our approach is feasible for the transcriptional analysis of a few cells in a cluster of intact plant cells without perturbing the viability of the non-targeted cells.

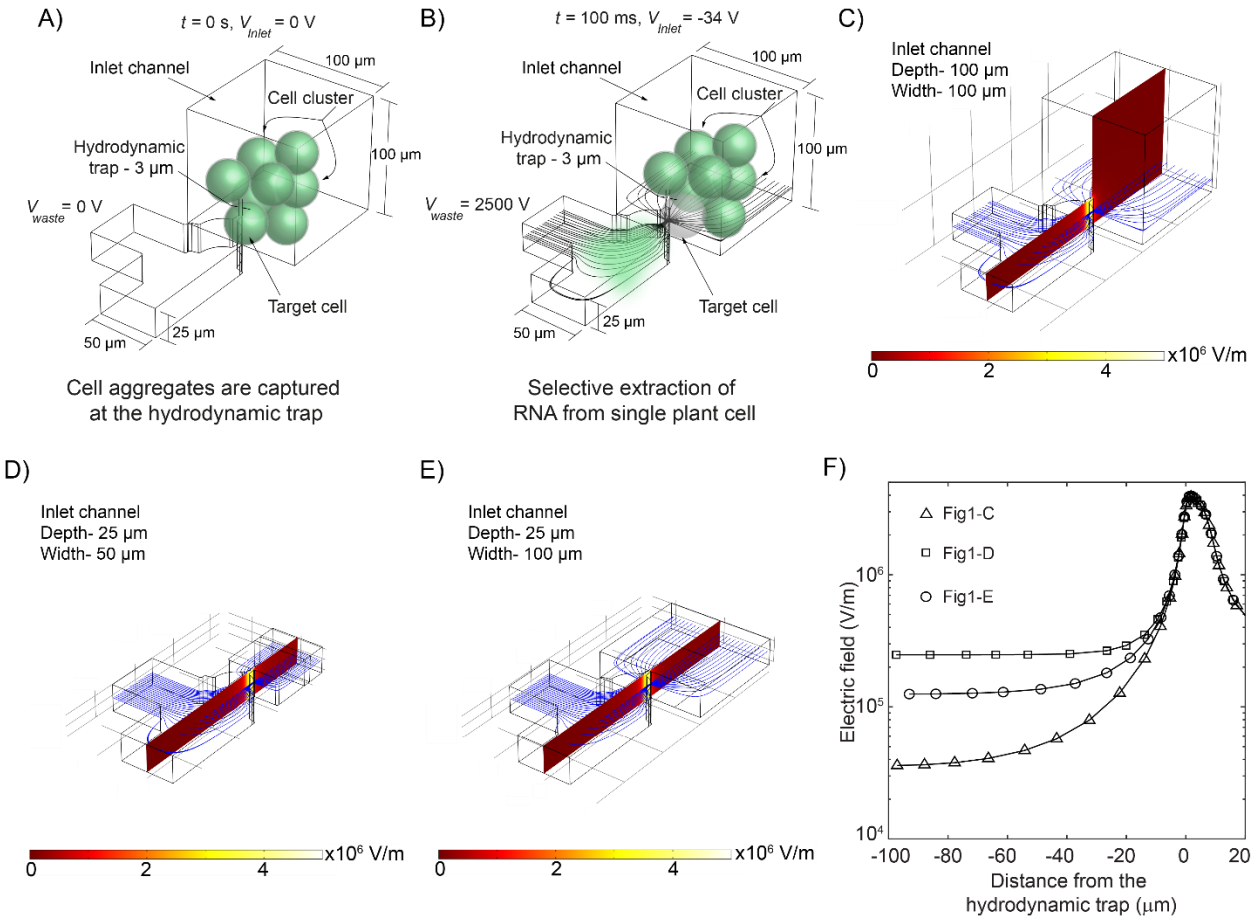

Figure 3.1 An overview of the selective permeabilization and extraction of cytosolic molecules from the targeted cell in intact cluster. (A, B) An intact cluster is captured at the hydrodynamic trap. The focused electric field is exerted to the targeted cell in the cluster by applying voltages to the end-channel electrodes immersed in reservoirs. (C-E) Effect of the electric field in different channel geometries. Blue lines show the electric field lines. (F) Electric field distribution at the hydrodynamic trap and inlet channel. The microchannel design of Fig. 3.1D was developed by Abdelmoez et al. (Abdelmoez et al., 2018)

3.2 Materials and methods

3.2.1 Plant cell culture and staining

We maintained the “deep” cells, which are suspension cell culture and derived from root cells of *Arabidopsis thaliana* in a culture media (Table 3.1) at 22°C, stirring at 120 rpm in dark and sub-cultured every 7 days. We maintained BY-2 (*Nicotiana tabacum*) in modified Linsmaier and Skoog medium (Table 3.2) at 27°C, stirring at 130 rpm in dark and sub-cultured every 7 days. We investigated the cell viability by staining the cells using Plant Cell Viability Assay Kit (PA0100-1KT, Sigma) with two fluorescence dyes: fluorescein diacetate (FDA), which is a membrane-permeable dye, and propidium iodide (PI), which is a membrane-impermeable dye, for 1-2 min at room temperature. We observed a strong correlation between the fresh weight(https://epd.brc.riken.jp/en/archives/2942) and the expression level of the *GAPC1* (glyceraldehyde-3-phosphate dehydrogenase C subunit 1) gene, which is a housekeeping gene and stable for protoplasting, with the day since a subculture (Fig. 3.2). To standardize the experiment, we thus used cells on day 3-4, filtering them with a 70 μm cell strainer (352350, Falcon). We picked the cells negative for the PI staining with a micropipette and transferred to a fresh culture media containing PI. Immediately before each experiment, we suspended a single cluster of cells in a 100-μl droplet of the cell buffer and then hand-picked the cluster under an optical microscope with a micropipette. We followed a similar procedure for the experiment with a single protoplast.

Table 3.1 The culture media for deep cells. Dissolve the substances in the table in distilled water and adjust pH to 5.8 with 1 M KOH and fill up to 1000 ml.

Chemical	For 1000 ml culture media
Murashige and Skoog basal salt mixture (M5524, Sigma)	4.33 g
Myo-inositol (I7508-50G Sigma) 2wt%, nicotinic acid (N0761-100G) 0.02wt%, pyridoxine hydrochloride (P6280-25G) 0.02wt%, and Thiamine hydrochloride (T1270-25G Sigma) 0.2 wt%	10 ml
2,4-Dichlorophenoxyacetic acid (D7299-100G Sigma) (stock solution: 100 mg/l)	10 ml
KH_2PO_4 (P5655-100G, Sigma) (stock solution: 100 g/l)	3.4 ml
Sucrose (196-00015, Wako)	30 g

Table 3.2 The culture media for BY-2 cells. Dissolve the above substances in distilled water and adjust pH to 5.8 with 1 M KOH and fill up to 1000 ml.

Chemical	For 1000 ml culture media
Murashige and Skoog basal salt mixture (392-00591, Wako)	1 liter packet
KH_2PO_4 (P5655-100G, Sigma) 80 mg/ml	2.5 ml
Thiamine hydrochloride (T1270-25G Sigma) 0.4 mg/ml, Myo-Inositol (I7508-50G Sigma) 40 mg/ml	2.5 ml
2,4-Dichlorophenoxyacetic acid (D7299-100G Sigma) (stock solution: 0.2 mg/ml)	1 ml
Sucrose (196-00015 Wako)	30 g

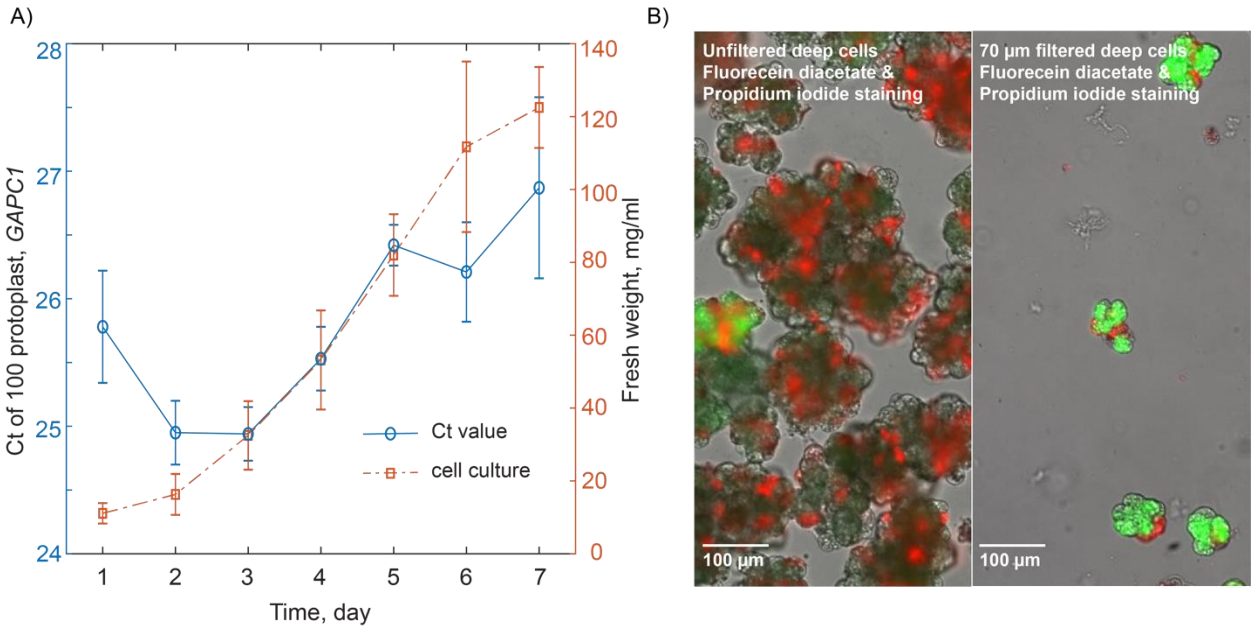

Figure 3.2 Quality control of the plant cell samples. A) Fresh weight (mg/ml) of deep cell culture and GAPC1 expression in 100 protoplasts on different day since sub-culture. B) Effect of filtration on the viability of deep cells with a 70-µm mesh filter. Deep cells were dual stained with FDA (false color, green) and PI (false color, red) before and after filtration.

3.2.2 Protoplast preparation

To prepare protoplasts, we took 1 ml of the cell culture suspension, allowed the cells to settle, and removed the supernatant by pipetting. We then added 1 ml of 0.4 M mannitol solution (M1902-500G, Sigma-Aldrich) and incubated the cells for 10 min. We discarded the supernatant and then added the cells to 5 ml of a protoplast media (the culture media Table SI1 with 0.4 M mannitol) supplemented with 0.4 µg/ml of pectolyase Y-23 (633-05013, Kyowa Kasei) and 10 mg/ml of cellulase Onozuka RS (Yakult Pharmaceutical industry). We incubated the cells for 3 hours at room temperature with mild stirring. We washed the protoplasts three times with the protoplast media and removed the supernatant after centrifugation at 94 × g for 3 min at 4°C. We finally re-suspended the protoplasts in the protoplast media and stored at 4°C until further use.

3.2.3 Fabrication of microchannel

We fabricated a two-layered mold for the microchannel with the following procedure (Fig. 3.3 and 3.4). We first patterned a chromium thin film on a glass substrate as the geometry of the first layer of the mold with a standard UV-lithography. Next, we coated the entire surface of the chromium film with an adhesive layer of SU-8 3005 (MicroChem), curing it with UV-exposure and heating. We fabricated the 25 μm-thick structure as the first layer of the mold, including the structure of a hydrodynamic trap (3 μm-wide and 5 μm-long) with SU-8 3025 (MicroChem) using the pattern in the chromium thin film at the UV-exposure. Notably, the UV-exposure through the chromium thin film on the glass substrate was the key to fabricate the high aspect-ratio geometry of the hydrodynamic trap by eliminating the air gap between the photomask and the surface of the photoresist in standard photolithography. We fabricated the 100 μm-thick structure as the second layer of the mold, including the geometry of the inlet region with SU-8 3050 over the first layer using a standard UV-lithography (see Fig. 3.3 for the geometry of the microchannel). We produced microchannel superstructures in polydimethylsiloxane (PDMS, Sylgard 184; Dow Corning, Midland, USA) by molding. We punched the reservoirs at the inlet, waste, and outlet terminals and then bonded with a pre-cleaned glass substrate (S1112, Matsunami) using plasma treatment.

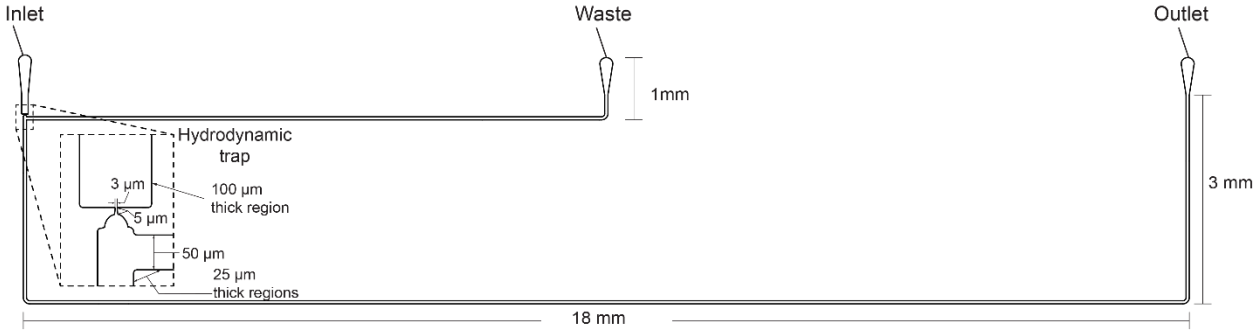

Figure 3.3 The geometry of the microchannel

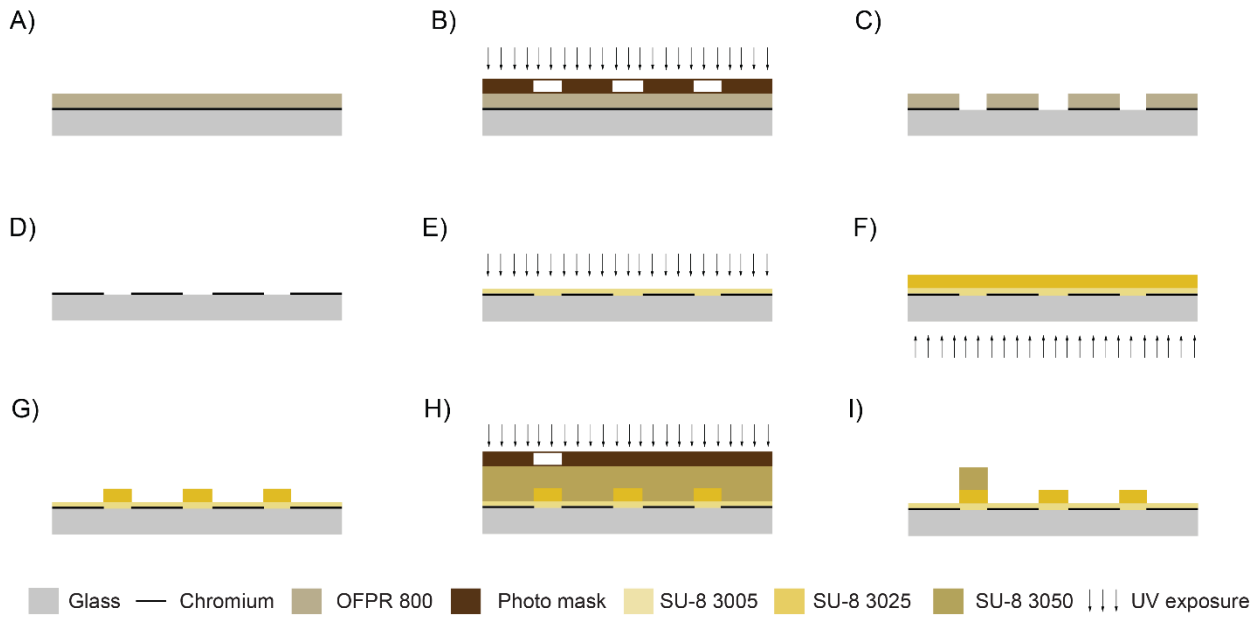

Figure 3.4 Schematic representation of fabrication of microchannel mold

3.2.4 ITP buffers

The leading electrolytes (LE) were 50 mM Tris and 25 mM HCl containing 0.4% poly(vinylpyrrolidone) (PVP) (calculated pH of 8.1). The trailing electrolyte (TE) were 50 mM imidazole, 25 mM HEPES, 0.4% PVP (calculated pH of 7.6) and 0.25 mg/ml bovine serum albumin (BSA). The cell buffer contained 50 mM imidazole, 25 mM HEPES, 175 mM sucrose, and 0.25 mg/ml BSA. We used a TE containing 0.34 M mannitol and a cell buffer containing 0.3 M mannitol for protoplasts.

3.2.5 Microfluidic protocol for extracting cytosolic molecules from targeted cells in a cluster of intact plant cells by electrical permeabilization and ITP-aided extraction

We washed the microchannel sequentially with 1 M NaOH, 1 M HCl, and nuclease-free water, all containing 0.1% Triton X-100. We then prefilled the microchannels with the LE and TE buffers and induced a pressure-driven flow from the inlet and outlet reservoirs toward the waste reservoir by dispensing 8.5 µl of fresh LE and TE buffers at the outlet and inlet reservoirs,

respectively (See Fig. 3.3 for the entire geometry of the microchannel). We then loaded a cluster of intact plant cells suspended in a 1 μl of the cell buffer and captured it at the hydrodynamic trap by mild vacuuming from the waste reservoir. We added 3.2 μl of TE buffer to the waste reservoir to stop the pressure-driven flow. We placed platinum electrodes (300 μm in diameter) at the inlet, waste, and outlet reservoirs, and then applied a pulsed voltage for lysis followed by DC voltage for the extraction of molecules as summarized in Table 3.3. We tested various pulsed voltages to control the number of lysing cells in a cluster. During step 2 for the extraction, we monitored the migration of the ITP interface via the current measurement, which attained a steady-state in about 100-120 s.

Table 3.3 voltage conditions and duration for RNA extraction from intact plant cell, protoplast and mammalian cells

	Inlet voltage, V	Waste voltage, V	Outlet voltage, V	Duration, s
Pulsed voltage for lysis	-2 to -38	120 to 2700	0	0.01 to 1
*Pushing voltage	-136 to -1364	-270 to -2700	0	0.01 to 1
*Resting pulse	0	0	0	1
Step 1 for extraction	-150	-170	0	40
Step 2 for extraction	-350	-510	0	160

* optional

3.2.6 Off-chip RT-qPCR analysis of extracted RNA

For off-chip analysis on the extracted RNA, we dispensed 10 µl of LE in the waste reservoir to prevent backflow from the outlet reservoir and then transferred the solution in the outlet reservoir to a fresh microfuge tube with a standard micropipette. We also analyzed the cluster retained at the hydrodynamic trap to evaluate cell quality, transferring 1 µl solution, including the retained cluster, to a fresh microfuge tube with a standard micropipette. We performed RT-qPCR targeting *GAPC1* with RNA-to-Ct (4392938, Thermo Fisher Scientific) and TaqMan gene expression assay (At02230057_g1, Thermo Fisher Scientific).

3.3 Results and discussion

3.3.1 Three-dimensional focusing of electric field targeting cells in a cluster

To exert focused electric field selectively to the targeted cells in a cluster, we designed the microchannel integrated with a hydrodynamic trap (3-µm wide and 25-µm deep) and a 100-µm wide and 100-µm deep inlet channel (Fig. 3.1). The inlet channel had a larger cross-section than the other parts of the microchannel (25 µm depth and 50 µm width) (See Fig. 3.3 for the entire microchannel). This design effectively increased the local electric field at the hydrodynamic trap while significantly reduced that in the inlet channel (Fig. 3.1C). We explored the importance of the channel design for focusing the electric field by performing numerical analyses with a microchannel integrated with different-sized inlet channels (Figs. 3.1D and E). In comparison to the microchannels with a uniform depth of 25 µm, the present design offered a significant reduction of the electric field in the inlet channel, i.e., demonstrating one order of magnitude higher focusing power of the electric field with the three-dimensional geometry by reducing the electric field in the inlet channel (Fig. 3.1F).

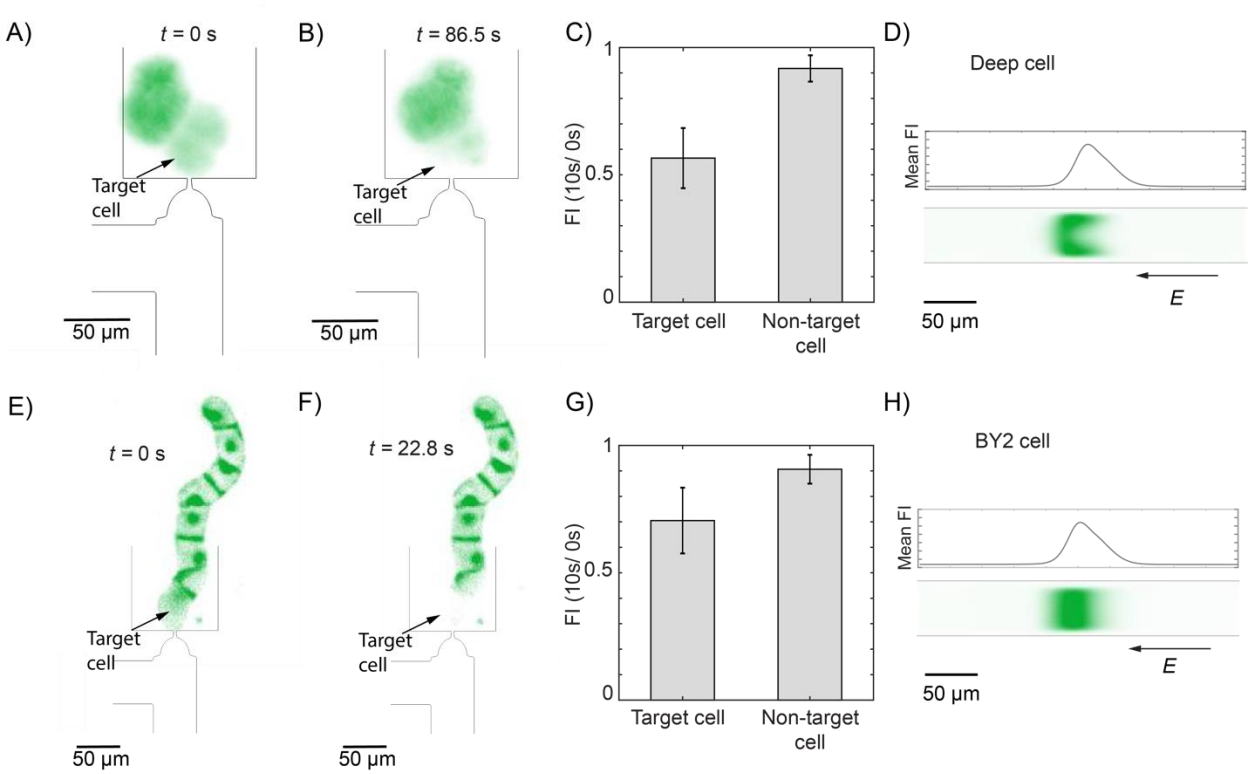

Figure 3.5 Extraction of FDA from a targeted cell in intact plant cluster. (A, B) Typical fluorescence images (false color) of deep cells in the 100-µm wide and 100-µm deep inlet channel before and after electrophoretic extraction of FDA. (C) Relative fluorescence intensities of targeted and non-targeted deep cells comparing before and after the application of the electric field. The regions of interest in the measurement were manually defined. (D) On-chip fluorescence images of extracted FDA at the LE-TE interface (false color) from intact deep cell. (E, F) Typical fluorescence images (false color) of BY-2 cells in the 100-µm wide and 100-µm deep inlet channel before and after electrophoretic extraction of FDA. (G) Relative fluorescence intensities of targeted and non-targeted BY2 cells comparing before and after the application of the electric field. (H) On-chip fluorescence images of extracted FDA at the LE-TE interface (false color) from intact BY-2 cell.

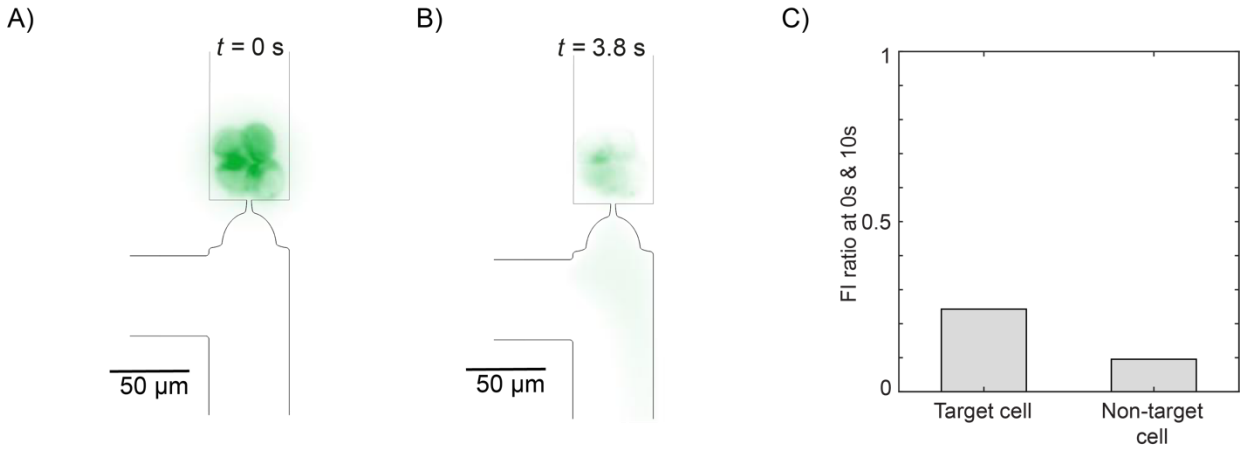

Figure 3.6 *(A, B) Typical fluorescence images (false color) of deep cells in the 50-μm wide and 45-μm deep inlet channel before and after electrophoretic extraction of FDA. (C) Relative fluorescence intensities of targeted and non-targeted cells comparing before and after the application of the electric field.*

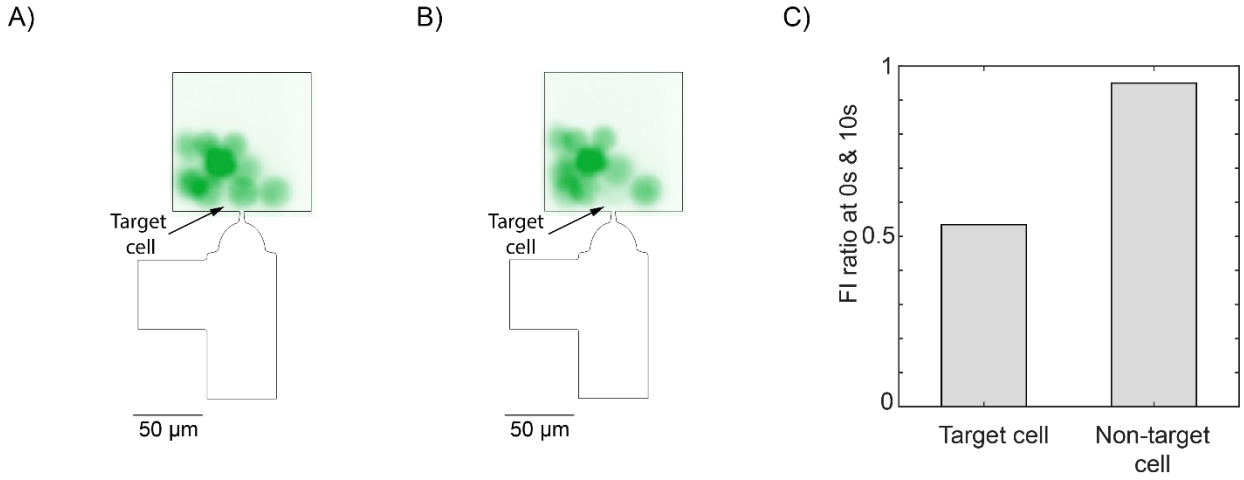

Figure 3.7 *Selective extraction of FDA from a single K562 cell in a cluster of intact cells.*

As supported by the numerical analysis, the focused electric field with three-dimensional geometry enabled the selective extraction of molecules from the targeted cell in intact plant cluster (Fig. 3.5). Figures 3.5A and B show representative images of FDA extraction from a targeted cell in the deep cells at the hydrodynamic trap by applying the DC electric field (Step1 and Step2 for extraction, Table 3.3). FDA fluorescence in cells indicated the viability of cells via esterase activity and

membrane integrity of the cells. We observed the significant reduction in the fluorescence of the FDA specifically in the targeted cell, which was physically contacted with the hydrodynamic trap, after the application of the focused electric field for 10 s (Fig. 3.5C). We observed the ITP focusing of the extracted FDA, as shown in Fig. 3.5D, supporting the successful extraction of FDA molecules from a targeted cell. For reference, we performed an identical experiment using a microchannel with a 50 μm wide and 45 μm deep inlet channel (Fig. 3.6). The microchannel was incapable of selective extraction of FDA from the targeted cell because of the insufficient focusing of the electric field, further supporting the importance of the inlet channel design.

Our approach offered the selective extraction of molecules from a targeted cell in a cluster with various morphologies and cell types. Figures 3.5 E-H show the extraction of the FDA from a tobacco BY-2 cell, which had a distinct cluster morphology than the deep cells. Our approach also enabled the selective extraction of calcein molecules from a targeted cell in a cluster of K562 cells (human leukemia cell line) without a cell wall (Fig. 3.7), suggesting the applicability of our approach to the mammalian cells.

3.3.2 Pulsed electric field for permeabilizing the cell wall

We next sought for the electric field condition that enables the extraction of RNA molecules from a cluster of intact plant cells. Our preliminary experiments found that the electric field created only with steps 1 and 2 summarized in Table 3.3 was insufficient to permeabilize the cell wall for extracting the RNA molecules. We here hypothesized that the cell wall physically hindered the migration of RNA molecules, which were bigger than FDA molecules. We reasoned that an intense electric field could further permeabilize the cell wall and enable extracting RNA molecules. To balance between sufficient permeabilization of the cell wall with suppressing the influence on the non-targeted cells, we developed a voltage sequence that combined a pulsed

electric field for permeabilizing a cell wall of a targeted cell with the DC electric field for the selective extraction of RNA molecules as summarized in Table 3.3.

We here evaluated the various conditions of the pulsed electric field by measuring the number of influenced cells in an intact cluster, identifying the influenced cells by PI staining after applying the pulsed voltage (before the application of the DC electric field). Our data uncovered that both the intensity and the duration of the pulsed electric field were keys to control the number of influenced cells (Fig. 3.8A). The number of influenced cells increased as increasing either duration or intensity of the pulsed electric field (Fig. 3.8B). We summarized the results with the mean number of influenced cells by performing the experiment more than three trials per condition. Notably, BY-2 cells showed qualitatively similar results to the deep cells despite the distinct morphology of the cluster, suggesting that the focused electric field created by the hydrodynamic trap offered the robust applicability to various cluster morphologies (Figs. 3.8C and D). We note that the pulsed electric field sometimes induced bubble generation at the hydrodynamic trap. However, the bubbles immediately disappeared for the rapid heat dissipation in the microfluidic system and showed no significant influence on the ITP-aided extraction by monitoring the current.

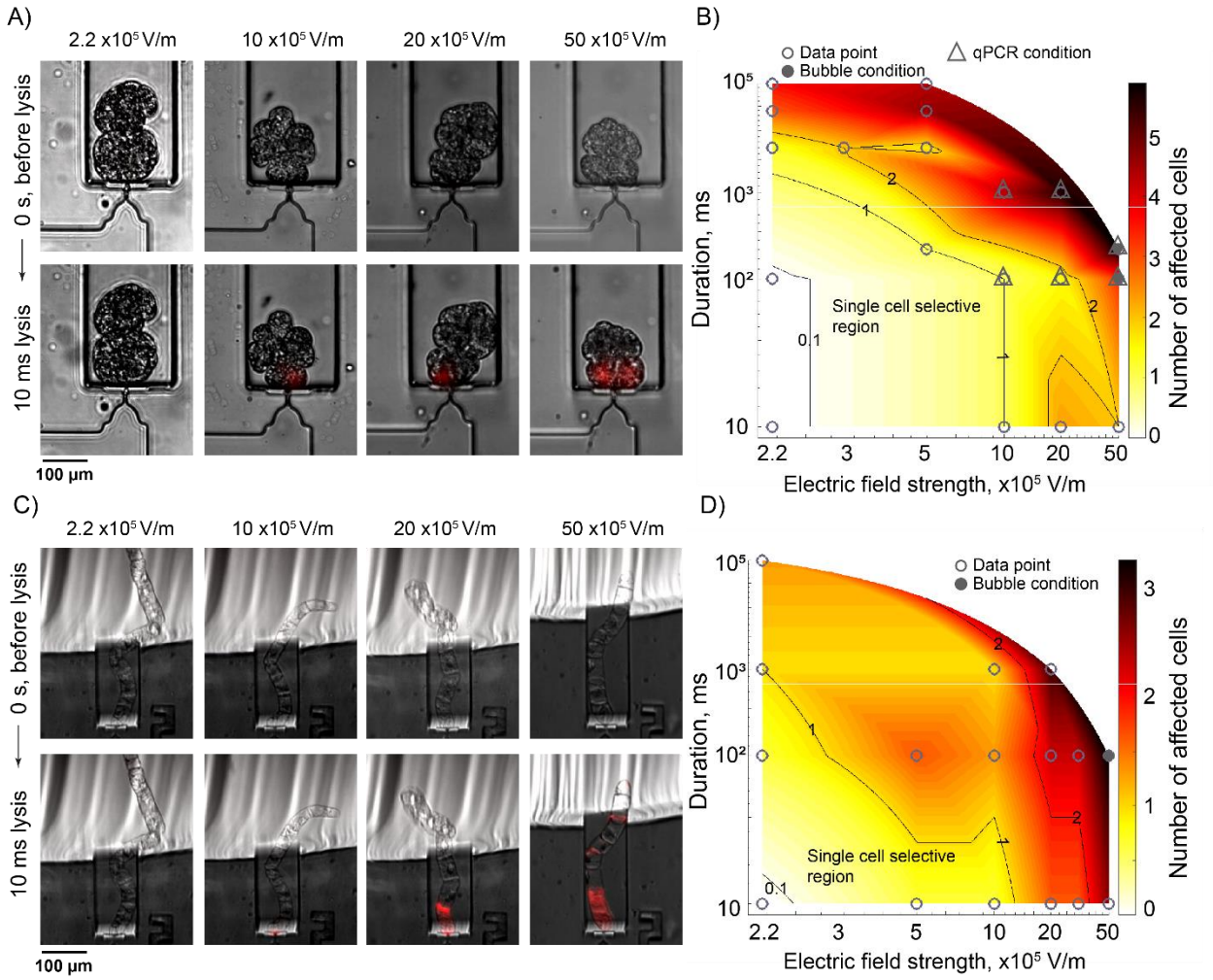

Figure 3.8 *Effects of the pulsed electric field in different plant species. (A) Merged images (bright field and fluorescence of PI staining) of deep cells before and after the cell lysis with various pulsed electric fields. (B) A contour plot shows the mean number of deep cells affected by the pulsed electric field under various conditions. (C) Merged images of BY-2 cells before and after the application of various pulsed electric fields. (D) A contour plot shows the number of BY-2 cells affected by the pulsed electric field under various conditions.*

3.3.3 Visualization and quantification of extracted RNA

To quantify the amount of extracted RNA molecules from plant cells via on-chip fluorescence measurement, we leveraged the focusing power of ITP to increase the local concentration of extracted RNA molecules in the LE-TE interface in the microchannel (Shintaku et al., 2014). We show representative images of extracted RNA molecules stained with SYBR Green II (Thermo Fisher Scientific) in Fig. 3.9A. We observed a stronger fluorescence in the ITP zone with a cluster at the hydrodynamic trap than that without a cluster. We note that our ITP protocol sometimes resulted in segregated peaks of RNA molecules, which were likely 18S and 28S ribosomal RNA molecules. To quantify the total amount of the extracted RNA molecules, we integrated the fluorescence signal in the LE-TE interface and summarized it as Fig. 3.9B. Despite the relatively low signal-to-noise ratio (11.8, (mean of background-subtracted intensity) / (standard deviation of background-subtracted intensity of negative control)) in this measurement, we could observe non-negligible fluorescence signals when applying the pulsed electric field of 46×10^5 V/m for 0.01-0.3 s to an intact deep cell in a cluster. The amount of the extracted RNA molecules from intact deep cells was smaller than that from a single protoplast, implying that the cell wall still hindered the RNA molecules from translocating though it.

To further confirm the extraction of RNA molecules, we performed off-chip RT-qPCR with the solution extracted from the outlet reservoir targeting *GAPC1*. Figure 3.9C shows that the protocol with the pulsed electric field successfully extracted RNA molecules from the intact deep cells, while not without the pulsed electric field. The values of *Ct* decreased as increasing the intensity of the pulsed electric field. To evaluate the amount of RNA, we here defined the equivalent number of cells that scaled the amount of the extracted RNA by the amount of RNA in a single protoplast (Fig. 3.9D). The results clearly showed that the amount of extracted RNA

increased as increasing the intensity of the pulsed electric field, suggesting the importance of the pulsed voltage for the RNA extraction. To estimate the number of cells that underwent the extraction of RNA molecules, we leveraged Fig. 3.8B, including the conditions of the pulsed electric field with triangle symbols. We hypothesized the expected numbers of cells influenced by the pulsed electric field were 1 ± 0, 1.5 ± 0.9, and 3.3 ± 0.9 for 10×10^5, $20\times10^{5,}$ and 50×10^5 V/m, respectively, out of 6 ± 2.7 cells in a cluster of cells.

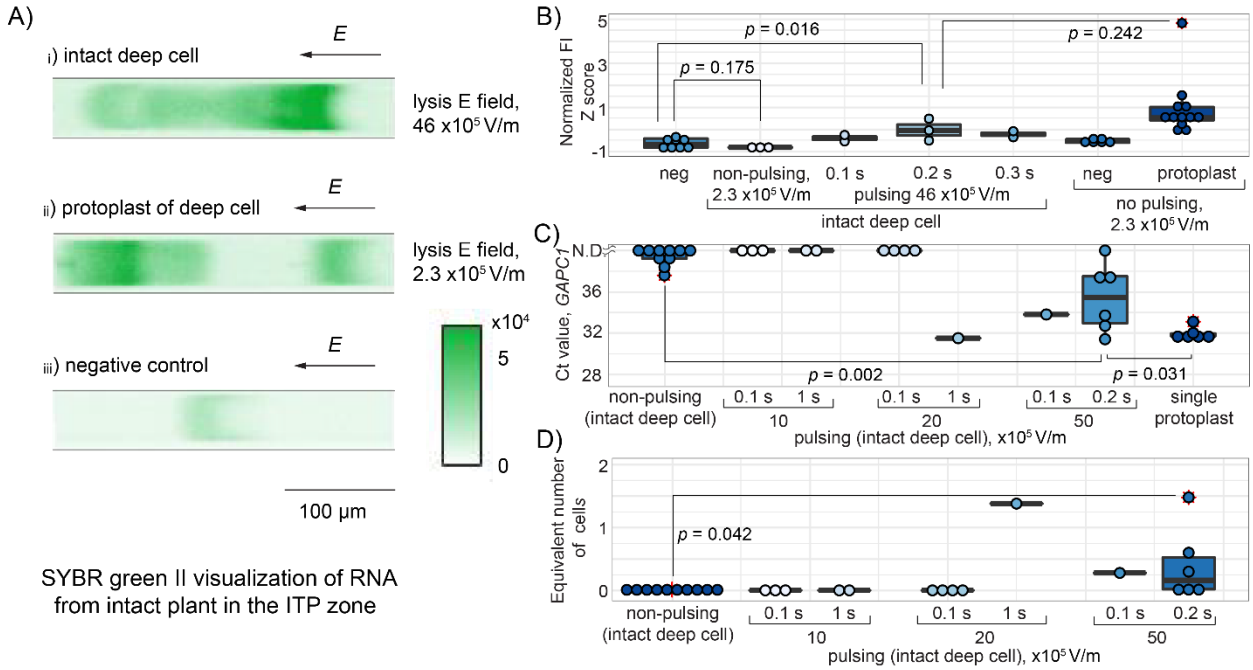

Figure 3.9 *Extracting RNA molecules from a few targeted cells in an intact cluster of deep cells. (A) Typical fluorescence images of RNA extracted and focused at the LE-TE interface of ITP from (i) intact deep cell, (ii) protoplast, and (iii) negative control, respectively. (B) Normalized fluorescence intensities of RNA stained with SYBR green II extracted from intact deep cells and protoplasts using z-score. (C) Off-chip RT-qPCR analyses on the extracted RNA molecules targeting GAPC1. N.D. indicates no amplification within 40 PCR cycles. (D) The equivalent number of cells estimates the relative amount of the extracted RNA to the amount of RNA in protoplast using GAPC1 on the basis of delta Ct.*

3.4 Summary

We have demonstrated the use of the focused electric field for permeabilizing the cell wall of a few cells in a cluster of intact plant cells and extracted cytosolic molecules from the targeted cells with maintaining the viability of non-targeted cells in the cluster. The approach leveraged the hydrodynamic trap to isolate an intact cluster of interest and to create the focused electric field by confining the path of the ionic current for the selective permeabilization and extraction. The approach offered about the 5 min workflow for extracting cytosolic molecules and outputting them to off-chip analyses without any enzymatic reactions. Specifically, we tested the approach by applying to two types of model plants, which had distinct cluster morphologies, as well as a mammalian cell line, demonstrating the broad applicability of our microfluidic approach. Leveraging the focusing power of ITP, we also demonstrated the on-chip fluorescence measurement of the extracted molecules from the targeted cells. We quantified the extracted amount of RNA via on-chip fluorescence microscopy under various conditions of electric fields. We uncovered that the intense pulsed electric field was essential to permeabilize the cell wall of the targeted cells and to extract the cytoplasmic RNA.

Our microfluidic approach has some advantages over capillary-based approaches. The system can readily offer the multimodal analysis of fluorescence microscopy of cells, electrophoresis of the extracted molecules as well as integration with off-chip analyses such as RT-qPCR. Although the throughput of this particular design is limited, tens of clusters can be rapidly processed by integrating the multiple hydrodynamic traps in the microchannel, for which our group is currently working. We provided a landscape of conditions of the pulsed electric field for controlling the number of influenced cells in an intact cluster, where we characterized the conditions by the intensity and duration of the pulsed electric field at the hydrodynamic trap. The

knowledge on the electric field of pulsing for permeabilization and DC for extraction is not limited to the microfluidics but can be applicable to capillary-based approaches by relating the electric field strength at the tip of the capillary.

Although the current design has a limitation for the size of the processing clusters by the size of the inlet channel, it can be easily modified for the bigger sized clusters by increasing the cross-section of the inlet channel. This modification has no influence on the intensity of the focused electric field at the hydrodynamic trap, while it further suppresses the influence on the non-targeted cells by reducing the electric field in the inlet channel.

4

Conclusion

We developed two independent microfluidic approaches to evaluate gene expression in single animal cells as well as plant cells at reduced perturbation. We employed a reverse crosslinking agent to fix animal cells and demonstrated the sub-cellular fractionation of RNA from a fixed single cell. For plant cell, we designed and fabricated a microchannel capable of three-dimensional focusing of electric field to exhibit a direct extraction of cytoplasmic molecules from an intact plant cell. We have demonstrated the usefulness of our approaches with wide applications.

4.1 ITP based RNA extraction from DSP fixed single cells

In this study, we performed a preliminary screening of cell fixation protocols using methanol, ethanol and DSP for superior adaptation on our electrokinetic platform. We extracted RNA from a single fixed cell using electrical lysis and ITP protocol and analyzed the extracted RNA by RTqPCR targeting *GAPDH* gene. We found that the cytoplasmic RNA extracted from DSP-fixed cells had comparable extraction efficiency as that of fresh cells. We used DSP-fixed cells to perform further investigations.

We performed a deeper examination of the DSP-fixed cells and found that the conventional DSP fixation protocol had exhibited a massive leakage of cell contents from the DSP-fixed cells.

We analyzed the DSP fixed cells with calcein, Hoechst and trypan blue staining and uncovered a significant loss of calcein molecules within 12 hours of fixation. We also found a substantial leakage of RNA molecules, a critical cross contaminant in single cell RNA sequencing procedures. We modified the DSP fixation to minimize the leakage of cell contents. We supplemented the cell storage buffer with sucrose and found that sucrose prolonged the cell membrane integrity resulting in a significant retention of cell contents for extended durations.

We performed on-chip reverse crosslinking of DSP fixation using DTT and found that DTT addition in the TE buffer improved ITP-based RNA extraction. Although there was a general reduction of the extraction of RNA as the DSP-fixed cells aged.

We effectively integrated the on-chip electro-kinetic protocol with off-chip single cell RNA sequencing technology. We demonstrated the strength of our methodology by drawing parallel comparison with fresh cell RNA sequencing data. We analyzed the two subcellular fraction of RNA obtained from the same single cell. We performed 8 single cell experiments and obtained 16 sub-cellular fractions with 100% success rate. We compared the extracted RNA and retained RNA fractions of DSP-fixed single cell to fresh cells for cDNA yield, number of detected genes, Pearson correlation of TPM, correlation between RTqPCR & RNA sequencing and overall gene expression. We detected 2000 gene/DSP-fixed cell (retained fraction) and obtained a Pearson correlation above 0.6 implying repeatability and sensitivity. We observed length bias in mRNA extraction from DSP-fixed cells and saw that shorter transcripts (< 1 kb) exhibited 85% extraction relative to fresh cell and the longer transcripts (> 1 kb) showed 46% relative extraction to fresh cell. However, the average gene expression of DSP fixed cells was highly consistent with fresh cell demonstrating the effectiveness our protocol.

4.2 Extraction of charged molecules from single cells of plants in intact clusters using three-dimensional focusing of electric field

We demonstrated a direct extraction of cell contents from an intact plant cell using a modified microchannel. The channel geometry of the chip used to extract RNA from DSP-fixed animal cell had narrow dimensions to accommodate plant cells which are larger in size and also occurs in clusters. We modified the dimensions of the inlet channel by increasing the depth and width from 25 µm to 100 µm and 50 µm to 100 µm. We retained the rest of the channel geometry to be same as the previous design. We performed numerical and experimental analysis with different channel geometries and found that our new design exhibited significant increase of local electric field at the hydrodynamic trap and critically reduced the electric field effect away from the trap. This resulted in reduced electric field effect on non-target cells and similar effect was observed using cluster of mammalian cells.

Next, we demonstrated selective extraction of small molecules from the target single cell in a cluster. We used FDA stained plant cells and confirmed the extraction by focusing the extracted FDA molecules in the ITP zone. We used intact plant of different species having different morphology to exhibit the wide applicability of our approach. We could extract small molecules using a low electric field strength (2.3×10^5 V/m).

We found that electric field used to extract small molecules from an intact plant was not sufficient enough to permeabilize the cell wall to extract large molecules like RNA. We studied the effect of electric field strength and duration on the intact plant clusters. We created a landscape of conditions and found that both the electric field strength and duration are critical parameters in measuring the number of cells affected. We visualized the RNA extracted from an intact using SYBR Green II of RNA focused in the ITP zone. We further examined the extracted RNA by RTqPCR targeting *GAPC1*. We effectively detected *GAPC1* gene in the RNA extracted from intact

deep cell and compared with *GAPC1* levels in a single protoplast. We successfully demonstrated for the first time the extraction of charged molecules from single cells in intact plant cluster using three-dimensional focusing of electric field in a microchannel.

4.3 Recommendations for future studies

We envision to extend our methodologies of animal cell fixation to adapt to parallel processing of many single cells, which might potentially take longer cell loading time and biologically challenging cell samples like samples having shorter gene expression response time. For plant cells, we will demonstrate differential gene expression using single-cell RNA sequencing technology and extend our protocol to study multiple targets in a single plant cell.

Bibliography

Abdallah, B. Y., Horne, S. D., Stevens, J. B., Liu, G., Ying, A. Y., Vanderhyden, B., & Heng, H. H. (2013). Single cell heterogeneity: why unstable genomes are incompatible with average profiles. *Cell Cycle*, 12(23), 3640. doi:10.4161/cc.26580

Abdelmoez, M. N., Iida, K., Oguchi, Y., Nishikii, H., Yokokawa, R., Kotera, H., & Shintaku, H. (2018). SINC-seq: correlation of transient gene expressions between nucleus and cytoplasm reflects single-cell physiology. *Genome Biol*, 19(1), 66. doi:10.1186/s13059-018-1446-9

Abdelmoez, M. N., Oguchi, Y., Ozaki, Y., Yokokawa, R., Kotera, H., & Shintaku, H. (2020). Distinct kinetics in electrophoretic extraction of cytoplasmic RNA from single cells. *Anal Chem*, 92(1), 1485. doi:10.1021/acs.analchem.9b04739

Alles, J., Karaiskos, N., Praktiknjo, S. D., Grosswendt, S., Wahle, P., Ruffault, P. L., & Rajewsky, N. (2017). Cell fixation and preservation for droplet-based single-cell transcriptomics. *BMC Biol*, 15(1), 44. doi:10.1186/s12915-017-0383-5

Altschuler, S. J., & Wu, L. F. (2010). Cellular heterogeneity: do differences make a difference? *Cell*, 141(4), 559. doi:10.1016/j.cell.2010.04.033

Angermueller, C., Clark, S. J., Lee, H. J., Macaulay, I. C., Teng, M. J., Hu, T. X., & Reik, W. (2016). Parallel single-cell sequencing links transcriptional and epigenetic heterogeneity. *Nat Methods*, 13(3), 229. doi:10.1038/nmeth.3728

Attar, M., Sharma, E., Li, S., Bryer, C., Cubitt, L., Broxholme, J., & Bowden, R. (2018). A practical solution for preserving single cells for RNA sequencing. *Sci Rep*, 8(1), 2151. doi:10.1038/s41598-018-20372-7

Birnbaum, K., Shasha, D. E., Wang, J. Y., Jung, J. W., Lambert, G. M., Galbraith, D. W., & Benfey, P. N. (2003). A gene expression map of the Arabidopsis root. *Science*, 302(5652), 1956. doi:10.1126/science.1090022

Darmanis, S., Sloan, S. A., Croote, D., Mignardi, M., Chernikova, S., Samghababi, P., & Quake, S. R. (2017). Single-cell RNA-seq analysis of infiltrating neoplastic cells at the migrating front of human glioblastoma. *Cell Rep*, 21(5), 1399. doi:https://doi.org/10.1016/j.celrep.2017.10.030

Darmanis, S., Sloan, S. A., Zhang, Y., Enge, M., Caneda, C., Shuer, L. M., & Quake, S. R. (2015). A survey of human brain transcriptome diversity at the single cell level. *Proc Natl Acad Sci*, 112(23), 7285. doi:10.1073/pnas.1507125112

Denyer, T., Ma, X., Klesen, S., Scacchi, E., Nieselt, K., & Timmermans, M. C. P. (2019). Spatiotemporal developmental trajectories in the Arabidopsis root revealed using high-throughput single-cell RNA sequencing. *Dev Cell*, 48(6), 840. doi:10.1016/j.devcel.2019.02.022

Dobin, A., Davis, C. A., Schlesinger, F., Drenkow, J., Zaleski, C., Jha, S., & Gingeras, T. R. (2013). STAR: ultrafast universal RNA-seq aligner. *Bioinformatics*, 29(1), 15.

doi:10.1093/bioinformatics/bts635

Elowitz, M. B., Levine, A. J., Siggia, E. D., & Swain, P. S. (2002). Stochastic gene expression in a single cell. *Science*, 297(5584), 1183. doi:10.1126/science.1070919

Espina, V. A., Liotta, L. A., & Mueller, C. (2013). One-step cell and tissue preservative for morphologic and molecular analysis. US Patent Application(13/575,001), US 2013/0137094A0137091

Gierahn, T. M., Wadsworth, M. H., 2nd, Hughes, T. K., Bryson, B. D., Butler, A., Satija, R., & Shalek, A. K. (2017). Seq-Well: portable, low-cost RNA sequencing of single cells at high throughput. *Nat Methods*, 14(4), 395. doi:10.1038/nmeth.4179

Guillaumet-Adkins, A., Rodriguez-Esteban, G., Mereu, E., Mendez-Lago, M., Jaitin, D. A., Villanueva, A., & Heyn, H. (2017). Single-cell transcriptome conservation in cryopreserved cells and tissues. *Genome Biol*, 18(1), 45. doi:10.1186/s13059-017-1171-9

Han, F., Wang, Y., Sims, C. E., Bachman, M., Chang, R., Li, G. P., & Allbritton, N. L. (2003). Fast electrical lysis of cells for capillary electrophoresis. *Anal Chem*, 75(15), 3688. doi:10.1021/ac0341970

Han, X., Wang, R., Zhou, Y., Fei, L., Sun, H., Lai, S., & Guo, G. (2018). Mapping the Mouse Cell Atlas by Microwell-Seq. *Cell*, 172(5), 1091-1107.e1017. doi:https://doi.org/10.1016/j.cell.2018.02.001

Hu, P., Zhang, W., Xin, H., & Deng, G. (2016). Single cell isolation and analysis. *Front Cell Dev Biol*, 4, 116.

Hu, Y., An, Q., Sheu, K., Trejo, B., Fan, S., & Guo, Y. (2018). Single Cell Multi-Omics Technology: Methodology and Application. *Front Cell Dev Biol*, 6(28). doi:10.3389/fcell.2018.00028

Islam, S., Zeisel, A., Joost, S., La Manno, G., Zajac, P., Kasper, M., & Linnarsson, S. (2014). Quantitative single-cell RNA-seq with unique molecular identifiers. *Nat Methods*, 11(2), 163. doi:10.1038/nmeth.2772

Ito, H., Tanaka, M., Zhou, Y., Nashimoto, Y., Takahashi, Y., Ino, K., & Shiku, H. (2017). Continuous collection and simultaneous detection of picoliter volume of nucleic acid samples using a mille-feuille probe. *Anal Bioanal Chem*, 409(4), 961. doi:10.1007/s00216-016-0006-y

Jaitin, D. A., Kenigsberg, E., Keren-Shaul, H., Elefant, N., Paul, F., Zaretsky, I., & Amit, I. (2014). Massively parallel single-cell RNA-seq for marker-free decomposition of tissues into cell types. *Science*, 343(6172), 776. doi:10.1126/science.1247651

Jean-Baptiste, K., McFaline-Figueroa, J. L., Alexandre, C. M., Dorrity, M. W., Saunders, L., Bubb, K. L., & Cuperus, J. T. (2019). Dynamics of gene expression in single root cells of Arabidopsis thaliana. *Plant Cell*, 31(5), 993. doi:10.1105/tpc.18.00785

Khnouf, R., Shore, S., Han, C. M., Henderson, J. M., Munro, S. A., McCaffrey, A. P., & Santiago, J. G. (2018). Efficient production of on-target reads for small RNA sequencing of single cells using modified adapters. *Anal Chem*, 90(21), 12609. doi:10.1021/acs.analchem.8b02773

Klein, Allon M., Mazutis, L., Akartuna, I., Tallapragada, N., Veres, A., Li, V., & Kirschner, Marc W. (2015). Droplet Barcoding for Single-Cell Transcriptomics Applied to Embryonic Stem Cells. *Cell*, 161(5), 1187. doi:https://doi.org/10.1016/j.cell.2015.04.044

Kubo, M., Nishiyama, T., Tamada, Y., Sano, R., Ishikawa, M., Murata, T., & Hasebe, M. (2019). Single-cell transcriptome analysis of Physcomitrella leaf cells during reprogramming using microcapillary manipulation. *Nucleic Acids Res*, 47(9), 4539. doi:10.1093/nar/gkz181

Kuriyama, K., Shintaku, H., & Santiago, J. G. (2015). Isotachophoresis for fractionation and recovery of cytoplasmic RNA and nucleus from single cells. *Electrophoresis*, 36(14), 1658. doi:10.1002/elps.201500040

Kuriyama, K., Shintaku, H., & Santiago, J. G. (2016a). Protocol for microfluidic system to automate the preparation and fractionation of the nucleic acids in the cytoplasm versus nuclei of single cells. *Bio-protocol*, 6. doi:10.21769/BioProtoc.1844

Lee, J., Hyeon, D. Y., & Hwang, D. (2020). Single-cell multiomics: technologies and data analysis methods. *Exp Mol Med*, 52(9), 1428. doi:10.1038/s12276-020-0420-2

Levy, Sasha F. (2016). Cellular Heterogeneity: Benefits besides bet-hedging. *Curr Biol*, 26(9), R355. doi:https://doi.org/10.1016/j.cub.2016.03.034

Li, B., & Dewey, C. N. (2011). RSEM: accurate transcript quantification from RNA-Seq data with or without a reference genome. *BMC Bioinformatics*, 12, 323. doi:10.1186/1471-2105-12-323

Lorenzo Tejedor, M., Mizuno, H., Tsuyama, N., Harada, T., & Masujima, T. (2009). Direct single-cell molecular analysis of plant tissues by video mass spectrometry. *Anal Sci*, 25(9), 1053. doi:10.2116/analsci.25.1053

Lorenzo Tejedor, M., Mizuno, H., Tsuyama, N., Harada, T., & Masujima, T. (2012). In situ molecular analysis of plant tissues by live single-cell mass spectrometry. *Anal Chem*, 84(12), 5221. doi:10.1021/ac202447t

Macaulay, I. C., Haerty, W., Kumar, P., Li, Y. I., Hu, T. X., Teng, M. J., & Voet, T. (2015). G&T-seq: parallel sequencing of single-cell genomes and transcriptomes. *Nat methods*, 12(6), 519. doi:10.1038/nmeth.3370

Macosko, E. Z., Basu, A., Satija, R., Nemesh, J., Shekhar, K., Goldman, M., & McCarroll, S. A. (2015). Highly parallel genome-wide expression profiling of individual cells using nanoliter droplets. *Cell*, 161(5), 1202. doi:10.1016/j.cell.2015.05.002

McClain, M. A., Culbertson, C. T., Jacobson, S. C., Allbritton, N. L., Sims, C. E., & Ramsey, J. M. (2003). Microfluidic devices for the high-throughput chemical analysis of cells. *Anal Chem*, 75(21), 5646. doi:10.1021/ac0346510

Nashimoto, Y., Echigo, M., Ino, K., & Shiku, H. (2019). Site-specific cytosol sampling from a single cell in an intact tumor spheroid using an electrochemical syringe. *Anal Chem*, 91(14), 8772-8776. doi:10.1021/acs.analchem.9b02062

Nashimoto, Y., Takahashi, Y., Zhou, Y., Ito, H., Ida, H., Ino, K., & Shiku, H. (2016). Evaluation of mRNA localization using double barrel scanning ion conductance microscopy. *ACS Nano*, 10(7), 6915. doi:10.1021/acsnano.6b02753

Navin, N. E. (2015). The first five years of single-cell cancer genomics and beyond. *Genome Res*, 25(10), 1499. doi:10.1101/gr.191098.115

Newman, J. R. S., Ghaemmaghami, S., Ihmels, J., Breslow, D. K., Noble, M., DeRisi, J. L., & Weissman, J. S. (2006). Single-cell proteomic analysis of S. cerevisiae reveals the architecture of biological noise. *Nature*, 441(7095), 840. doi:10.1038/nature04785

Panina, Y., Karagiannis, P., Kurtz, A., Stacey, G. N., & Fujibuchi, W. (2020). Human Cell Atlas and cell-type authentication for regenerative medicine. *Exp Mol Med*, 52(9), 1443. doi:10.1038/s12276-020-0421-1

Papalexi, E., & Satija, R. (2017). Single-cell RNA sequencing to explore immune cell heterogeneity. *Nat Rev Immunol*, 18, 35. doi:10.1038/nri.2017.76

Peterson, V. M., Zhang, K. X., Kumar, N., Wong, J., Li, L., Wilson, D. C., & Klappenbach, J. A. (2017). Multiplexed quantification of proteins and transcripts in single cells. *Nat Biotechnol*, 35(10), 936. doi:10.1038/nbt.3973

Prestrelski, S. J., Tedeschi, N., Arakawa, T., & Carpenter, J. F. (1993). Dehydration-induced conformational transitions in proteins and their inhibition by stabilizers. *Biophys J*, 65(2), 661. doi:10.1016/S0006-3495(93)81120-2

Raj, A., & van Oudenaarden, A. (2008). Nature, nurture, or chance: stochastic gene expression and its consequences. *Cell*, 135(2), 216. doi:https://doi.org/10.1016/j.cell.2008.09.050

Rogacs, A., Marshall, L. A., & Santiago, J. G. (2014). Purification of nucleic acids using isotachophoresis. *J Chromatogr A*, 1335, 105. doi:10.1016/j.chroma.2013.12.027

Rosenberg, A. B., Roco, C. M., Muscat, R. A., Kuchina, A., Sample, P., Yao, Z., & Seelig, G. (2018). Single-cell profiling of the developing mouse brain and spinal cord with split-pool barcoding. *Science*, 360(6385), 176. doi:10.1126/science.aam8999

Roy, A. L., Conroy, R., Smith, J., Yao, Y., Beckel-Mitchener, A. C., Anderson, J. M., & Wilder, E. L. (2018). Accelerating a paradigm shift: the common fund single cell analysis program. *Sci Adv*, 4(8), eaat8573. doi:10.1126/sciadv.aat8573

Rye, D. B., Saper, C. B., & Wainer, B. H. (1984). Stabilization of the tetramethylbenzidine (TMB) reaction product: application for retrograde and anterograde tracing, and combination with immunohistochemistry. *J Histochem Cytochem*, 32(11), 1145. doi:10.1177/32.11.6548485

Ryu, K. H., Huang, L., Kang, H. M., & Schiefelbein, J. (2019). Single-cell RNA sequencing resolves molecular relationships among individual plant cells. *Plant Physiol*, 179(4), 1444. doi:10.1104/pp.18.01482

Saliba, A.-E., Westermann, A. J., Gorski, S. A., & Vogel, J. (2014). Single-cell RNA-seq: advances and future challenges. *Nucleic Acids Res*, 42(14), 8845. doi:10.1093/nar/gku555

Saunders, A., Macosko, E. Z., Wysoker, A., Goldman, M., Krienen, F. M., de Rivera, H., & McCarroll, S. A. (2018). Molecular Diversity and Specializations among the Cells of the Adult Mouse Brain. *Cell*, 174(4), 1015.e1016. doi:https://doi.org/10.1016/j.cell.2018.07.028

Shalek, A. K., Satija, R., Adiconis, X., Gertner, R. S., Gaublomme, J. T., Raychowdhury, R., & Regev, A. (2013). Single-cell transcriptomics reveals bimodality in expression and splicing

in immune cells. *Nature*, 498, 236. doi:10.1038/nature12172

Shamir, M., Bar-On, Y., Phillips, R., & Milo, R. (2016). Snapshot: timescales in cell biology. *Cell*, 164(6), 1302. doi:10.1016/j.cell.2016.02.058

Shintaku, H., Nishikii, H., Marshall, L. A., Kotera, H., & Santiago, J. G. (2014). On-chip separation and analysis of RNA and DNA from single cells. *Anal Chem*, 86(4), 1953. doi:10.1021/ac4040218

Shulse, C. N., Cole, B. J., Ciobanu, D., Lin, J., Yoshinaga, Y., Gouran, M., & Dickel, D. E. (2019). High-throughput single-cell transcriptome profiling of plant cell types. *Cell Rep*, 27(7), 2241. doi:10.1016/j.celrep.2019.04.054

Stephenson, W., Donlin, L. T., Butler, A., Rozo, C., Bracken, B., Rashidfarrokhi, A., & Satija, R. (2018). Single-cell RNA-seq of rheumatoid arthritis synovial tissue using low-cost microfluidic instrumentation. *Nat Commun*, 9(1), 791. doi:10.1038/s41467-017-02659-x

Subramanian Parimalam, S., Oguchi, Y., Abdelmoez, M., Tsuchida, A., Ozaki, Y., Yokokawa, R., & Shintaku, H. (2018). Electrical lysis and RNA extraction from single cells fixed by dithio-bis(succinimidyl propionate). *Anal Chem*, 90, 12512. doi:10.1021/acs.analchem.8b02338

Svensson, V., Vento-Tormo, R., & Teichmann, S. A. (2018). Exponential scaling of single-cell RNA-seq in the past decade. *Nat Protoc*, 13(4), 599. doi:10.1038/nprot.2017.149

Tellez-Gabriel, M., Ory, B., Lamoureux, F., Heymann, M.-F., & Heymann, D. (2016). Tumour heterogeneity: the key advantages of single-cell analysis. *Int J Mol Sci*, 17(12), 2142. doi:10.3390/ijms17122142

Thomsen, E. R., Mich, J. K., Yao, Z., Hodge, R. D., Doyle, A. M., Jang, S., & Ramanathan, S. (2016). Fixed single-cell transcriptomic characterization of human radial glial diversity. *Nat Methods*, 13(1), 87. doi:10.1038/nmeth.3629

Torii, K., Inoue, K., Bekki, K., Haraguchi, K., Kubo, M., Kondo, Y., & Endo, M. (2019). Origination of the circadian clock system in stem cells regulates cell differentiation. *bioRxiv*, 710590. doi:10.1101/710590

Trapnell, C., Cacchiarelli, D., Grimsby, J., Pokharel, P., Li, S., Morse, M., & Rinn, J. L. (2014). The dynamics and regulators of cell fate decisions are revealed by pseudotemporal ordering of single cells. *Nat Biotechnol*, 32(4), 381. doi:10.1038/nbt.2859

Wu, A. R., Neff, N. F., Kalisky, T., Dalerba, P., Treutlein, B., Rothenberg, M. E., & Quake, S. R. (2014). Quantitative assessment of single-cell RNA-sequencing methods. *Nat Methods*, 11(1), 41. doi:10.1038/nmeth.2694

Wu, J., Suzuki, H., Zhou, Y. W., Liu, W., Yoshihara, M., Kato, M., & Nakashima, I. (2001). Cepharanthine activates caspases and induces apoptosis in Jurkat and K562 human leukemia cell lines. *J Cell Biochem*, 82(2), 200. doi:10.1002/jcb.1155

Xiang, C. C., Mezey, E., Chen, M., Key, S., Ma, L., & Brownstein, M. J. (2004). Using DSP, a reversible cross-linker, to fix tissue sections for immunostaining, microdissection and expression profiling. *Nucleic Acids Res*, 32(22), e185. doi:10.1093/nar/gnh185

Yang, E., van Nimwegen, E., Zavolan, M., Rajewsky, N., Schroeder, M., Magnasco, M., & Darnell,

J. E., Jr. (2003). Decay rates of human mRNAs: correlation with functional characteristics and sequence attributes. *Genome Res*, 13(8), 1863. doi:10.1101/gr.1272403

Zhang, X., Marjani, S. L., Hu, Z., Weissman, S. M., Pan, X., & Wu, S. (2016). Single-cell sequencing for precise cancer research: progress and prospects. *Cancer Res*, 76(6), 1305. doi:10.1158/0008-5472.can-15-1907

List of publications

Journal papers

1. Subramanian Parimalam, S., Oguchi, Y., Abdelmoez, M., Tsuchida, A., Ozaki, Y., Yokokawa, R., & Shintaku, H. (2018). Electrical lysis and RNA extraction from single cells fixed by dithio-bis(succinimidyl propionate). *Anal Chem*, 90, 12512. doi:10.1021/acs.analchem.8b02338
2. Subramanian Parimalam, S., Abdelmoez, M., Tsuchida, A., Sotta, N., Tanaka, M., Kuromori, T., Fujiwara, T., Hirai, M., Yokokawa, R., Oguchi, Y., & Shintaku, H. "Targeted permeabilization of cell wall and extraction of charged molecules from single cells in intact plant clusters using focused electric field". *Submitted (under review)*

Conference presentations and posters

1. Subramanian Parimalam, S., Sotta, N., Kuromori, T., Fujiwara, T., Yokoto Hirai, M., & Shintaku, H. "Extraction of RNA from an intact single plant cell with cell wall using focused electric field" in Proceedings of *IEEE International Symposium on Micro-NanoMechatronics and Human Science*, Nagoya University, Japan, 1-4 December (2019), 275.
2. Subramanian Parimalam, S., Sotta, N., Fujiwara, T., Yokoto Hirai, M., & Shintaku, H. "Selective and direct extraction of cytoplasmic RNA from single plant cell in an intact tissue via focused electric field" in Proceedings of *EMBO workshop on Single Cell Biology,* Tokyo, 20-22 May (2019).
3. Subramanian Parimalam, S., Oguchi, Y., Abdelmoez, M., Tsuchida, A., Ozaki, Y., Yokokawa, R., Kotera, H., & Shintaku, H. "Electrical cell lysis and isotachophoresis aided RNA extraction from fixed single cells" *The All-RIKEN Workshop,* Wakoshi, 14 December (2018).
4. Subramanian Parimalam, S., Oguchi, Y., Abdelmoez, M., Tsuchida, A., Ozaki, Y., Yokokawa, R., Kotera, H., & Shintaku, H. "Isotachophoresis-based RNA extraction from fixed single cells" in the Proceedings of the *Symposium on Micro-Nano Science and Technology, B Chem.*, vol. 2018.9, 30am3PN37, 30 October (2018). DOI: https://doi.org/10.1299/jsmemnm.2018.9.30am3PN37
5. Subramanian Parimalam, S., Oguchi, Y., Abdelmoez, M., Tsuchida, A., Ozaki, Y., Yokokawa, R., Kotera, H., & Shintaku, H. "Extraction and fractionation of RNA from fixed single cells" *TMN Poster Session,* Yamanaka, 28 September (2018).
6. Subramanian Parimalam, S., Kubo, M., Yokokawa, R., Kotera, H., and Shintaku, H. "Differentiating cell-cycle heterogeneity by pico-liter well based microRNA cytometry" *TM Network workshop,* Yamagata, 03 August (2016).
7. Subramanian Parimalam, S., Yokokawa, R., Kotera, H., & Shintaku, H. "Massively parallel quantification of miRNA in single cells via duplex-specific nuclease reaction in pico-liter wells" 2016 *International conference of Microfluidics, Nanofluidics, and Lab-on-a-chip*, Dalian, China, 10th June (2016), Track13-292, 287-288.
8. Subramanian Parimalam, S., Kubo, M., Yokokawa, R., Kotera, H., & Shintaku, H. "One step assay for miRNA quantification in single cells via duplex-specific nuclease induced signal amplification" *ナノミクス第3回若手研究者交流会*, Kyoto University, Katsura, 18 November (2015).